Engineered flavoproteins as bioorthogonal photo-triggers for the activation of metal-based anticancer prodrugs

Laura F. Mazzei,[a,b,c] Juan Gurruchaga-Pereda,[a] Álvaro Martínez,[b,c] Javier Calvo Martínez,[a] Luca Salassab,[c,d,*] and Aitziber L. Cortajarena[a,d,*]

[a.] Center for Cooperative Research in Biomaterials (CIC biomaGUNE), Basque Research and Technology Alliance (BRTA), Paseo de Miramon 194, Donostia-San Sebastián, 20014, Spain.
[b.] Donostia International Physics Center, Paseo Manuel de Lardizabal 4, Donostia-San Sebastián, 20018, Spain.
[c.] Polimero eta Material Aurreratuak: Fisika, Kimika eta Teknologia, Kimika Fakultatea, Euskal Herriko Unibertsitatea UPV/EHU, Paseo Manuel de Lardizabal 3, Donostia-San Sebastián, 20018, Spain.
[d.] Ikerbasque, Basque Foundation for Science, Bilbao, 48009, Spain.
[*]Corresponding authors: alcortajarena@cicbiomagune.es; lsalassa@dipc.org
[†] Footnotes relating to the title and/or authors should appear here.

A multifunctional hybrid constructed for controlling the delivery and activation of Pt anticancer agents in vitro is described herein. We employed consensus tetratricopeptide repeat protein (CTPR) for the covalent co-anchoring of riboflavin (photocatalyst) and a Pt(IV) prodrug complex. The Pt-loaded flavoprotein induced a 40% reduction in PANC-1 cell viability as a result of the photocatalytic formation of cisplatin.

Multifunctional hybrids[1] constructed by biomolecular templating are structures capable of performing complex activities depending on the nature of each component.[2] They are generally composed of a biomolecule that, mimicking the natural scaffolds,[3,4,5] displays multiple elements with a defined organization. Proteins are the most widely used templates, and in particular repeat proteins, since their repeated modular nature makes them ideal scaffolds for engineering.[6,7,8] Within these protein families, the consensus tetratricopeptide repeat proteins (CTPRs) are a helix-turn-helix motif of 34 amino acids that has successfully been implemented in the design and fabrication of protein-nanomaterial hybrids for different uses.[2] Only 8 residues have a key structural role to define the CTPR fold, hence leaving plenty of room for introducing sequence mutations capable of conferring diverse chemical and biological functions.[2] CTPRs have been shown to be robust platforms for the generation of systems that allow the templating of gold nanoparticles,[9] metallic nanoclusters,[10] redox active clusters,[11] carbon nanotubes and porphyrins,[12] among others. These hybrids have so far been studied for applications such as electroconductivity,[13] optics[14,15] catalysis and theranostics.[11,16] In light of their versatility and robustness, we were intrigued about the prospect of engineering CTPRs as platforms for controlling the activation and delivery of Pt(IV) prodrugs. These are among the most promising anticancer agents and have been extensively investigated, including in clinical trials, as convenient alternatives to clinically approved Pt(II) blockbuster drugs such as cisplatin, carboplatin and oxaliplatin.[17] Functionalization of metal complexes with short peptide sequences and anchoring to whole proteins and antibodies is a well-established strategy to improve the selectivity for cancerous tissues/cells and the effectiveness of these prospective chemotherapy agents.[18,19] For example, Kowol, Heffeter, and co-workers recently demonstrated that maleimido-functionalized Pt(IV) prodrugs effectively bind to human serum albumin available in the bloodstream, dramatically improving the pharmacokinetic profile and the antitumoral features of the complexes *in vivo*.[20,21] Engineered proteins, particularly CTPRs, are considered viable alternatives to other metallodrug protein-based carriers, such as antibodies, due to their robustness, ease of functionalization, and modular nature. In contrast, antibodies suffer from several disadvantages including high production and storage costs, limited stability, and low batch-to-batch reproducibility.[2]

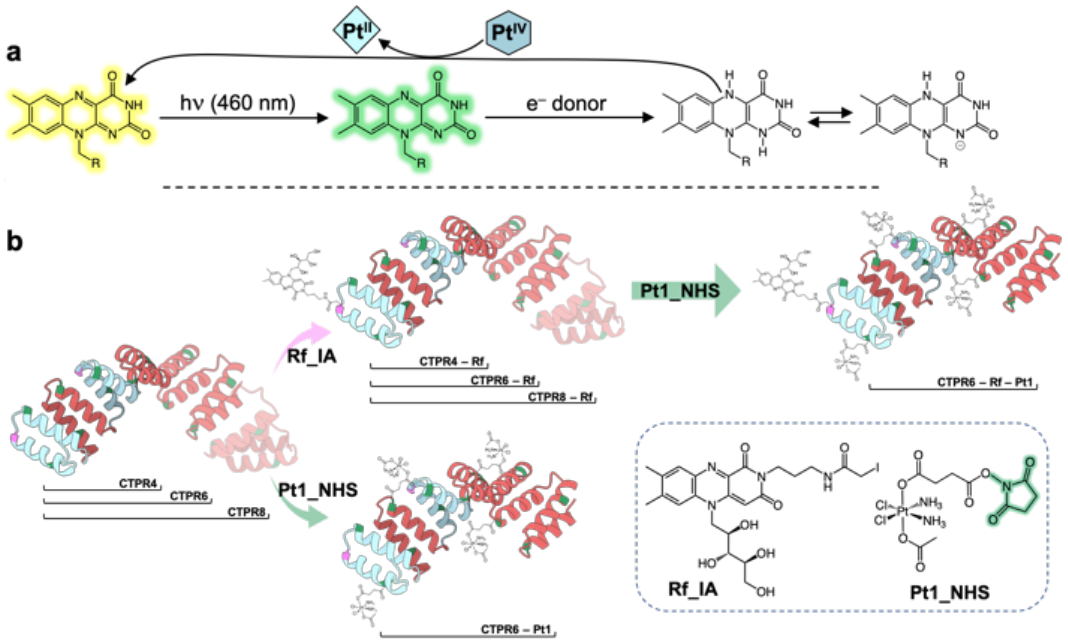

Fig. 1 (a) Flavin-mediated photocatalytic activation of Pt(IV) prodrugs. R = ribityl. (b) Bioconjugation scheme for the hybrids studied in this work. CTPR modules with a single cysteine at position 17 and wild-type modules are depicted in light blue and red, respectively. Cysteines used for coupling to **Rf-IA** are highlighted in pink, while lysine sites for coupling to **Pt1-NHS** are colored in green.

To this purpose, we aimed at integrating CTPRs with the photocatalytic activation of Pt(IV) complexes mediated by flavins that we recently reported.[22,23] Our previous work shows that flavin cofactors[24] and certain flavoproteins[23,25] can photocatalyze the conversion of Pt(IV) precursors into cisplatin and carboplatin with high efficiency and minimal light doses. This chemistry takes place in the presence of electron donors (e.g. NADH, amines, ascorbate) upon visible light excitation (460 nm). Under such conditions, the oxidized flavin (Fl) is reductively quenched to generate the flavin hydroquinone (FlH_2/FlH^-) which then prompts the Pt(IV) activation with bioorthogonal-like selectivity (Fig. 1a).[26]

In this contribution, we report on the design of new hybrid protein-based systems (**$CTPR_n$-Rf-Pt1**) composed of an iodoacetamide functionalized riboflavin (**Rf-IA**) and Pt prodrug (**Pt1-NHS**), both covalently anchored to CTPRs. In the studied assemblies, the riboflavin derivative simultaneously acts as photosensitizer and photocatalyst, while the Pt complex as substrate. We hypothesized that proteins could function as biomolecular scaffolds providing high biocompatibility and efficacy due to the co-immobilization of both components.

We employed three CTPR scaffolds with varying lengths and CTPR modules. Each scaffold is composed of a **CTPR4** module that alternates wild type (WT) and Cys modules — a CTPR module with a cysteine at position 17 to attach **Rf-IA** through cysteine-iodoacetamide coupling. **CTPR6** and **CTPR8** scaffolds integrate 2 and 4 additional WT modules, respectively. Lysine residues in the CTPR WT sequence were coupled with carboxyl-activated **Pt1-NHS** via amide formation (Fig. 1b). As detailed in Fig. S1 (ESI†), preparation of **CTPR-Rf-Pt1** started by synthesizing **Rf-IA** through a multi-step procedure.[27-30] The *cis,cis,trans*-[$Pt(NH_3)_2(Cl)_2(OCOCH_3)(O_2CCH_2CH_2CO_2H)$] complex (**Pt1**) was selected as prodrug. **Pt1** synthesis and activation with N-hydroxysuccinimide to afford **Pt1-NHS** was achieved by adapting the methodology previously reported in the literature[31-33] (Fig. S2, ESI†). Furthermore, we prepared the *cis,cis,trans*-[$Pt(NH_3)_2(Cl)_2(O_2CCH_2CH_2CO_2H)_2$] analogue (**Pt2**, Fig. S3, ESI†) bearing two succinate ligands in the axial position for comparison purposes. Our groups extensively employed this latter derivative as model substrate for studying flavin-catalyzed activation reactions of Pt anticancer drugs.[23,24,34,25] CTPR proteins modified with cysteines were recombinantly expressed and purified following methods previously reported by us (ESI†).[35,13]
After confirming its stability in PBS buffer (Fig. S4, ESI†), **Rf-IA** was conjugated to the three CTPRs (Fig. 2 and Fig. S5-S7, ESI†). Formation of **$CTPR_n$-Rfs** was first determined by the presence of a band with higher molecular weight compared to $CTPR_n$ in the electrophoresis gel (Fig. 2a). MALDI-TOF confirmed this result by elucidating the number of riboflavin molecules linked to the CTPRs. In the case of **CTPR6-Rf** (Fig. 2b), a peak was observed at a higher mass (29.5 kDa, blue plot marked by *) compared to the scaffold alone (29.0 kDa, gray plot marked by **), indicating the binding of a single

riboflavin to **CTPR6**. Similar results were obtained for **CTPR4** and **CTPR8** (Fig. S6b-S7b, ESI†). We compared circular dichroism (CD) spectra of CTPRs with the spectra of the **CTPR4-Rf**, **CTPR6-Rf**, and **CTPR8-Rf** in PB buffer. Overall, the CTPR secondary structure was unaltered after the coupling with **Rf-IA**, (Fig. 2c, Fig. S6c-S7c, ESI†), confirming, the robustness of the protein scaffolds upon functionalization with organic molecules,[13,12] and their suitability as platforms for drug delivery.

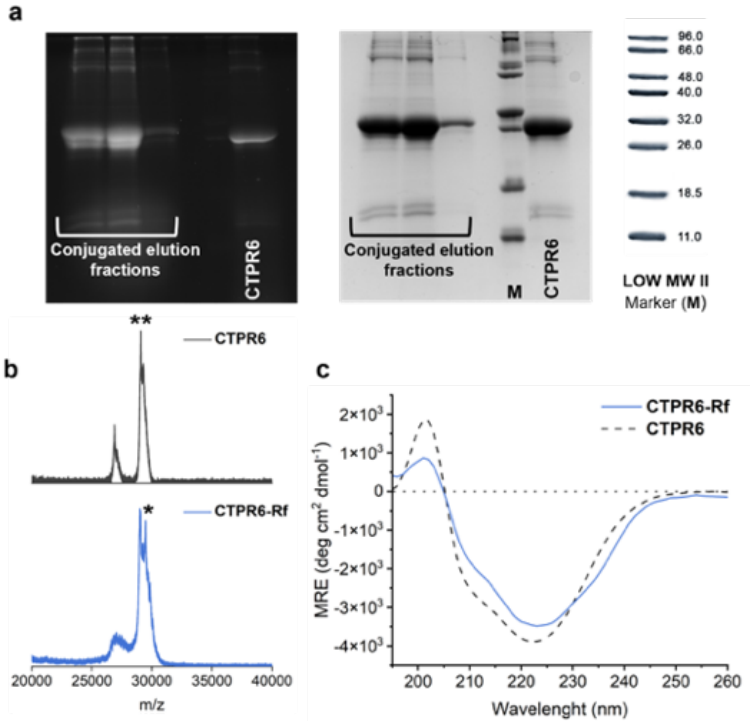

Fig. 2 Characterization of the **CTPR6-Rf** conjugate**.** (a) SDS-PAGE gel electrophoresis of the **CTPR6-Rf** conjugation elution fractions, **CTPR6** control and marker. The gel is imaged using UV light to monitor the fluorescence of riboflavin (left) and after Coomassie Blue staining of the proteins (right). (b) MALDI-TOF spectra of **CTPR6-Rf** and **CTPR6** control. Peak assignment: 29.0 kDa **CTPR6**, 29.5 kDa **CTPR6** (29.01 kDa) + **Rf** (MW_{Rf} = 474 Da, molecular weight without the leaving group, I). (c) CD spectra in PB buffer of **CTPR6-Rf** (blue solid line) and **CTPR6** (black dashed line) in the spectral region of the protein secondary structure absorption.

Next, we investigated how the protein conjugation affects the riboflavin photostability. To this aim, we compared the behavior of **Rf**, **FMN, Rf-IA,** and **CTPR$_n$-Rf** under blue light irradiation (460 nm, 3.5 mW/cm^2), observing a remarkable increase in stability for functionalized proteins in the first 20 min of light exposure (Fig. S8, ESI†). This effect could be attributed to the ability of the protein scaffold to protect the riboflavin moiety from the photodegradation. Previous work[22,36] demonstrated that photoredox catalytic efficiency of flavins can be enhanced by electron donors such as zwitterionic buffers (Fig. S8g-n, ESI†). Thus, the catalytic performance of **CTPR$_n$-Rf** towards the photoactivation of Pt(IV) prodrugs was assessed using **Pt2** as model substrate and MES (2-ethanesulfonic acid) as electron donor (18 mM, pH 6.4). Under these conditions, the reaction progress was monitored by ^{1}H-NMR following the release of the axial succinate ligands which involved the concomitant generation of cisplatin.[34] Results reported in Fig. S9 indicated that **CTPR6-Rf** was the best catalyst among the protein-conjugated riboflavins. Although less efficient than **FMN**, particularly at early light exposure points, **CTPR6-Rf** reached more than 50% substrate conversion after 20 min of blue light irradiation and a final 85% conversion after 45 min. Dark controls of **FMN** and **CTPR$_n$-Rf** showed that activation of **Pt2** did not occur within 48 hours (Fig. S10, ESI†), and direct light exposure did not significantly activate substrate (Fig. S11, ESI†).

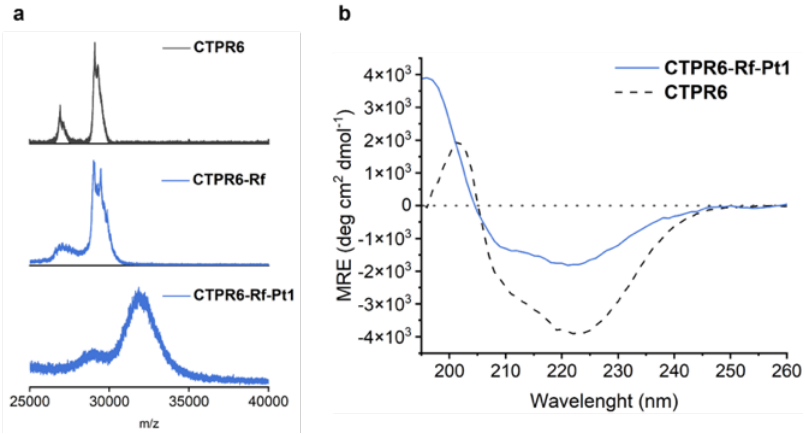

Fig. 3 Characterization of the **CTPR6-Rf-Pt1** hybrid. (a) MALDI-TOF spectra of **CTPR6-Rf-Pt1**, **CTPR6-Rf** and **CTPR6** (control). Peak assignment: 31.8 kDa **CTPR6-Rf-Pt1**, **CTPR6** (29.01 kDa) + **Rf** (MW_{Rf} = 474 Da, molecular weight without the leaving group, I) + 5 **Pt1** (MW_{Pt1} = 476 Da). (b) CD spectra in PB buffer of **CTPR6-Rf** (blue solid line) and **CTPR6** (black dashed line) in the spectral region of the protein secondary structure absorption.

Once demonstrated that **CTPR$_n$-Rf** can photocatalyze the activation of **Pt2**, we prepared a multicomponent hybrid system **CTPR$_n$-Rf-Pt**. In particular, we selected **CTPR6-Rf** among the different scaffolds for its superior catalytic performance, and **Pt1-NHS** for N-hydroxysuccinimide (NHS) ester-lysine coupling. **Pt1** was preferred over its **Pt2** analogue to avoid secondary reactions such as protein crosslinking, which could be favored by the presence of two reactive groups in the symmetric **Pt2**. ICP-MS and MALDI analysis confirmed that an average of 5 **Pt1** complexes were loaded on the **CTPR6-Rf-Pt1** complex (Fig. 3a). CD studies on **CTPR6-Rf-Pt1** showed that upon coupling with the Pt complex, the protein structure was mostly preserved (Fig. 3b), which stressed the robustness of the CTPR protein structure as already reported.[37] Furthermore, no changes in MALDI and CD spectra were observed after irradiation of **CTPR6-Rf-Pt1**, indicating that blue light does not substantially affect protein structure (Fig. S12, ESI†). Incubation experiments with GSH for 24 h confirmed the high stability of both the parent prodrug **Pt1** and **CTPR6-Rf-Pt1** in the dark (Fig. S13, ESI†).

Thereafter, we evaluated the efficacy of our conjugation strategy *in vitro* by testing **CTPR6-Rf-Pt1** in PANC-1 cancer cells. This cell line was selected based on previous studies performed by our group on cell lines derived from pancreas adenocarcinoma,[38] and the relevance of Pt drugs in treating this type of tumors.[39,40]

First, we evaluated the cytotoxicity in PANC-1 cells of **Pt1** compared to cisplatin, as positive control. The IC_{50} value for cisplatin was 56.9 µM, whereas **Pt1** prodrug was inactive (Fig. S14, ESI†). The capacity of **CTPR6-Rf-Pt1** to reduce cancer cell viability was then assessed in the dark and under light irradiation (3.5 mW/cm^2, alternating light on/off time periods), treating cells with different Pt concentrations (2.28 - 73.10 µM). According to data, the protein conjugate was nearly as effective as cisplatin in killing cells upon light activation (Fig. 4a), achieving a 40% reduction in cell viability at 73.10 µM. On the contrary, no toxic effects were observed in the dark for the protein conjugate, whereas cisplatin decreased the cell viability by approx. 30% (Fig. 4b). In addition to **CTPR6-Rf-Pt1**, we performed irradiation/dark experiments using single components and their combinations (Fig. S15, ESI†), finding that **CTPR6-Rf-Pt1** was overall more effective. Under light irradiation, **CTPR6** induced a slight decrease in cell viability (Fig. S16a, ESI†), likely due to the direct effect of blue light. In fact, it is known that light at this wavelength range is capable of triggering apoptosis in cancer cells (Fig. S16b, ESI†).[41] To further demonstrate this effect, we investigated a second light irradiation regime of 45 consecutive min of blue light (460 nm, 3.5 mW/cm^2), which expectedly was more stressful for the PANC-1 cells (Fig. S16c, ESI†). **CTPR6-Pt1** and **CTPR6-Rf** + free **Pt1** (1:28 Rf:Pt1) reduced cell viability to a lesser extent than the multicomponent hybrid, indicating that the flavin moiety plays a key role as phototrigger of the Pt(IV) reduction and that co-localization of **Rf** and **Pt1** is beneficial to improve the effectiveness of the flavin-mediated activation strategy within the cell. In **CTPR6-Rf-Pt1**, the transformation of the Pt prodrug into cisplatin is likely to occur due to endogenous electron donors present in the cell, since no external reductants (e.g. MES) are employed in these experiments, and light is administered only after cells are washed from the drugs, and the medium replaced (ESI†).

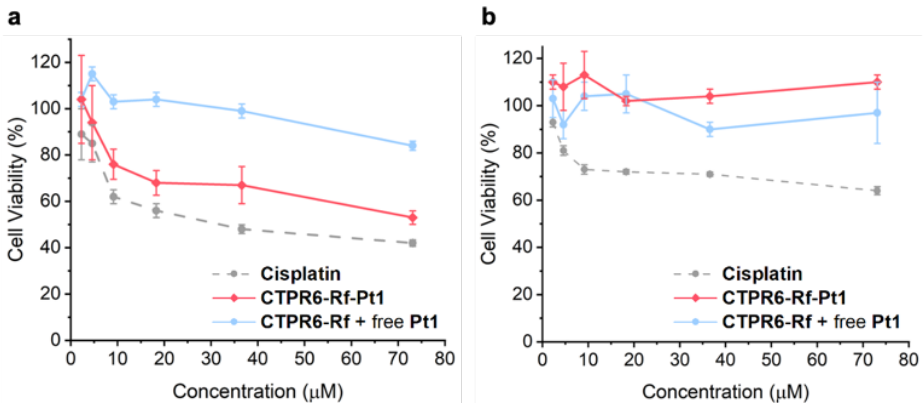

Fig. 4 Percentage cell viability in PANC-1 cancer cells following treatment with cisplatin (gray dashed line), **CTPR6-Rf-Pt1** (solid red line) and **CTPR6-Rf** + free **Pt1** (solid light blue line) (a) under light irradiation (45 min, light on/off regime, 460 nm, 3.5 mW/cm^2) and (b) in the dark.

The results reported here demonstrate that covalently functionalized CTPRs with riboflavin afford artificial flavoproteins capable of triggering the photocatalytic activation of a Pt(IV) anticancer complex. The versatility of the scaffold allows further derivatization by co-loading of metal-based prodrugs directly onto the protein, ultimately providing hybrid systems for the controlled delivery of Pt anticancer agents. Compared to related supramolecular platforms based on Au nanoparticles recently reported by us,[34] covalent anchoring of **Rf** and **Pt1** certainly represent a step forward in terms of biocompatibility and robustness. Nevertheless, to move **CTPR$_n$-Rf-Pt** towards *in vivo* studies, further optimization of their design and synthesis is fundamental. This will enable the assesment of their potential benefits in terms of drug pharmacokinetics and selective accumulation into tumors. In conclusion, photocatalytic activation of Pt drugs with CTPR-based flavoproteins may provide valuable solutions to minimize unwanted effects associated with these anticancer agents and achieve higher efficacy *in vivo*.

We acknowledge financial support from the Spanish State Research Agency (grants PID2019-109111RB-I00 and PID2019-111649RB-I00), LS thanks the Spanish Multi-MetDrugs network (RED2018-102471-T) for fruitful discussion. We thank Dr. Sara H. Mejías at IMDEA Nanociencia for the support with the proteins part, Juan Sanchez-Camacho Sanchez at DIPC for the organic synthesis. This work was performed under the Maria de Maeztu and Severo Ochoa Centres of Excellence Programme run by the Spanish State Research Agency, Grant No. MDM-2017-0720 (CIC biomaGUNE) and CEX2018-000867-S (DIPC).

Conflicts of interest

There are no conflicts to declare.

Notes and references

1 A. Beloqui and A. L. Cortajarena, *Curr. Opin. Struct. Biol.*, 2020, **63**, 74–81.
2 K. B. Uribe, E. Guisasola, A. Aires, E. López-Martínez, G. Guedes, I. R. Sasselli and A. L. Cortajarena, *Acc. Chem. Res.*, 2021, **54**, 4166–4177.
3 R. Chen, Q. Chen, H. Kim, K.-H. Siu, Q. Sun, S.-L. Tsai and W. Chen, *Curr. Opin. Biotechnol.*, 2014, **28**, 59–68.
4 C.-J. Chiang, L.-J. Lin, Z. W. Wang, T.-T. Lee and Y.-P. Chao, *Process Biochem.*, 2014, **49**, 1122–1128.
5 C. M. Spillmann and I. L. Medintz, *J. Photochem. Photobiol. C Photochem. Rev.*, 2015, **23**, 1–24.
6 S. H. Mejias, A. Aires, P. Couleaud and A. L. Cortajarena, in *Protein-based Engineered Nanostructures*, eds. A. L. Cortajarena and T. Z. Grove, Springer International Publishing, Cham, 2016, vol. 940, pp. 61–81.
7 E. R. G. Main, J. J. Phillips and C. Millership, *Biochem. Soc. Trans.*, 2013, **41**, 1152–1158.
8 F. Parmeggiani and P.-S. Huang, *Curr. Opin. Struct. Biol.*, 2017, **45**, 116–123.
9 S. H. Mejias, E. López-Martínez, M. Fernandez, P. Couleaud, A. Martin-Lasanta, D. Romera, A. Sanchez-Iglesias, S. Casado, M. R. Osorio, J. M. Abad, M. T. González and A. L. Cortajarena, *Nanoscale*, 2021, **13**, 6772–6779.
10 A. Aires, I. Llarena, M. Moller, J. Castro-Smirnov, J. Cabanillas-Gonzalez and A. L. Cortajarena, *Angew. Chem. Int. Ed.*, 2019, **58**, 6214–6219.
11 S. H. Mejias, Z. Bahrami-Dizicheh, M. Liutkus, D. J. Sommer, A. Astashkin, G. Kodis, G. Ghirlanda and A. L. Cortajarena, *Chem. Commun.*, 2019, **55**, 3319–3322.

12 J. López-Andarias, S. H. Mejías, T. Sakurai, W. Matsuda, S. Seki, F. Feixas, S. Osuna, C. Atienza, N. Martín and A. L. Cortajarena, *Adv. Funct. Mater.*, 2018, **28**, 1704031.
13 S. H. Mejías, J. López-Andarias, T. Sakurai, S. Yoneda, K. P. Erazo, S. Seki, C. Atienza, N. Martín and A. L. Cortajarena, *Chem. Sci.*, 2016, **7**, 4842–4847.
14 X. Wu, X. He, K. Wang, C. Xie, B. Zhou and Z. Qing, *Nanoscale*, 2010, **2**, 2244.
15 H. Hu, P. Huang, O. J. Weiss, X. Yan, X. Yue, M. G. Zhang, Y. Tang, L. Nie, Y. Ma, G. Niu, K. Wu and X. Chen, *Biomaterials*, 2014, **35**, 9868–9876.
16 A. Aires, D. Maestro, J. Ruiz del Rio, A. R. Palanca, E. Lopez-Martinez, I. Llarena, K. Geraki, C. Sanchez-Cano, A. V. Villar and A. L. Cortajarena, *Chem. Sci.*, 2021, **12**, 2480–2487.
17 Z. Xu, Z. Wang, Z. Deng and G. Zhu, *Coord. Chem. Rev.*, 2021, **442**, 213991.
18 S. M. Meier-Menches and A. Casini, *Bioconjug. Chem.*, 2020, **31**, 1279–1288.
19 V. del Solar and M. Contel, *J. Inorg. Biochem.*, 2019, **199**, 110780.
20 J. Mayr, P. Heffeter, D. Groza, L. Galvez, G. Koellensperger, A. Roller, B. Alte, M. Haider, W. Berger, C. R. Kowol and B. K. Keppler, *Chem. Sci.*, 2017, **8**, 2241–2250.
21 H. Schueffl, S. Theiner, G. Hermann, J. Mayr, P. Fronik, D. Groza, S. van Schonhooven, L. Galvez, N. S. Sommerfeld, A. Schintlmeister, S. Reipert, M. Wagner, R. M. Mader, G. Koellensperger, B. K. Keppler, W. Berger, C. R. Kowol, A. Legin and P. Heffeter, *Chem. Sci.*, 2021, **12**, 12587–12599.
22 S. Alonso-de Castro, E. Ruggiero, A. Ruiz-de-Angulo, E. Rezabal, J. C. Mareque-Rivas, X. Lopez, F. López-Gallego and L. Salassa, *Chem. Sci.*, 2017, **8**, 4619–4625.
23 S. Alonso-de Castro, A. L. Cortajarena, F. López-Gallego and L. Salassa, *Angew. Chem. Int. Ed.*, 2018, **57**, 3143–3147.
24 J. Gurruchaga-Pereda, V. Martínez-Martínez, E. Rezabal, X. Lopez, C. Garino, F. Mancin, A. L. Cortajarena and L. Salassa, *ACS Catal.*, 2020, **10**, 187–196.
25 J. Gurruchaga-Pereda, V. Martínez-Martínez, E. Formoso, O. Azpitarte, E. Rezabal, X. Lopez, A. L. Cortajarena and L. Salassa, *J. Phys. Chem. Lett.*, 2021, **12**, 4504–4508.
26 S. Scoditti, E. Dabbish, G. E. Pieslinger, E. Rezabal, X. Lopez, E. Sicilia and L. Salassa, *Phys. Chem. Chem. Phys.*, 2022, **24**, 5323–5329.
27 J. B. Metternich, S. Sagebiel, A. Lückener, S. Lamping, B. J. Ravoo and R. Gilmour, *Chem. - Eur. J.*, 2018, **24**, 4228–4233.
28 A. Y.-T. Huang, C.-H. Tsai, H.-Y. Chen, H.-T. Chen, C.-Y. Lu, Y.-T. Lin and C.-L. Kao, *Chem. Commun.*, 2013, **49**, 5784.
29 J. Alguacil, S. Defaus, A. Claudio, A. Trapote, M. Masides and J. Robles, *Eur. J. Org. Chem.*, 2010, **2010**, 3102–3109.
30 C. Garino, S. Ghiani, R. Gobetto, C. Nervi, L. Salassa, V. Ancarani, P. Neyroz, L. Franklin, J. B. Alexander Ross and E. Seibert, *Inorg. Chem.*, 2005, **44**, 3875–3879.
31 R. A. Alderden, M. D. Hall and T. W. Hambley, *J. Chem. Educ.*, 2006, **83**, 728.
32 K. M. Brière, R. Goel, F. H. Shirazi, D. J. Stewart and I. C. P. Smith, *Cancer Chemother. Pharmacol.*, 1996, **37**, 518–524.
33 H. Yao, Z. Xu, C. Li, M.-K. Tse, Z. Tong and G. Zhu, *Inorg. Chem.*, 2019, **58**, 11076–11084.
34 L. F. Mazzei, Á. Martínez, L. Trevisan, D. Rosa-Gastaldo, A. L. Cortajarena, F. Mancin and L. Salassa, *Chem. Commun.*, 2020, **56**, 10461–10464.
35 T. Kajander, A. L. Cortajarena and L. Regan, in *Protein Design*, Humana Press, New Jersey, 2006, vol. 340, pp. 151–170.
36 L. C. P. Gonçalves, H. R. Mansouri, S. PourMehdi, M. Abdellah, B. S. Fadiga, E. L. Bastos, J. Sá, M. D. Mihovilovic and F. Rudroff, *Catal. Sci. Technol.*, 2019, **9**, 2682–2688.
37 T. Kajander, A. L. Cortajarena, S. Mochrie and L. Regan, *Acta Crystallogr. D Biol. Crystallogr.*, 2007, **63**, 800–811.
38 S. Alonso-de Castro, A. Terenzi, S. Hager, B. Englinger, A. Faraone, J. C. Martínez, M. Galanski, B. K. Keppler, W. Berger and L. Salassa, *Sci. Rep.*, 2018, **8**, 17198.
39 M. T. Saung and L. Zheng, *Clin. Ther.*, 2017, **39**, 2125–2134.
40 G. K. Gresham, G. A. Wells, S. Gill, C. Cameron and D. J. Jonker, *BMC Cancer*, 2014, **14**, 471.
41 G. Yan, L. Zhang, C. Feng, R. Gong, E. Idiiatullina, Q. Huang, M. He, S. Guo, F. Yang, Y. Li, F. Ding, W. Ma, V. Pavlov, Z. Han, Z. Wang, C. Xu, B. Cai, Y. Yuan and L. Yang, *Int. J. Biochem. Cell Biol.*, 2018, **103**, 81–88.

Supporting Information

Engineered flavoproteins as bioorthogonal photo-triggers for the activation of metal-based anticancer prodrugs

Laura F. Mazzei,[a,b,c] Juan Gurruchaga-Pereda,[a] Álvaro Martínez,[b,c] Javier Calvo Martínez,[a] Luca Salassa[b,c,d,*] and Aitziber L. Cortajarena[a,d,*]

[a] *Center for Cooperative Research in Biomaterials (CIC biomaGUNE), Basque Research and Technology Alliance (BRTA), Paseo de Miramon 194, Donostia-San Sebastián,20014, Spain.*
[b] *Donostia International Physics Center, Paseo Manuel de Lardizabal 4, Donostia-San Sebastián, 20018, Spain.*
[c] *Ikerbasque, Basque Foundation for Science, Bilbao, 48009, Spain.*
[d] *Polimero eta Material Aurreratuak: Fisika, Kimika eta Teknologia, Kimika Fakultatea, Euskal Herriko Unibertsitatea UPV/EHU, Paseo Manuel de Lardizabal 3, Donostia-San Sebastián, 20018, Spain.*

1. General methods

Materials. Chemicals, solvents and deuterated solvents for NMR were obtained from Merck and used as purchased without further purification. Ultrapure water was deionised and filtered with a Millipore milliQ system.
Column chromatography was performed with silica gel employing Macherey-Nagel Kieselgel 60 with particles sizes of 0.063–0.2 mm (gravity).

NMR spectroscopy. NMR spectra for characterization work were acquired on a Bruker 500 MHz Ultra Shield and Bruker Furier 300 MHz spectrometer. Spectra were calibrated using residual solvent signals according to previously reported values.[1]

UV-Vis spectroscopy. UV-Vis spectra were acquired with Biotek Synergy H1 microplate reader, NanoDrop Spectrophotometer ND-1000 and NanoDrop One^C Spectrophotometer. For the microplate reader measurements, 96 well UV flat bottom MicrotitorPlates (Thermo Fisher) were used. For both NanoDrop instruments, the measurements were performed loading 3.5 µl of sample.

Circular dichroism (CD). CD was used to determine the secondary structure of the CTPR units. CD was performed using a Jasco J-1500 spectropolarimeter. A quartz cuvette (0.1 mm path length) was used. The CD spectra were acquired at 1 nm increments and 2 seconds average time over a wavelength range of 190 to 260 nm.

Mass spectrometry.
ESI-MS. ESI (Electrospray ionization) mass spectra were recorded on an Agilent Technologies 1100 Series system equipped with a binary pump (G1312A) and MSD SL Trap mass spectrometer (G2445D SL) with ESI source from solutions in methanol or acetonitrile and 0.1% formic acid.

MALDI-TOF MS. The proteins and the organic compounds were analyzed using MALDI-TOF MS UltrafleXtreme III (Bruker) mass spectrometer. 3-(4-hydroxy-3,5-dimethoxyphenyl)prop-2-enoic acid was used as matrix at 10 mg/ml dissolved in a 70% acetonitrile and 0.1% TFA solution for proteins samples, 2,5-dihydroxybenzoic acid was used as matrix at 20 mg/ml dissolved in 70% acetonitrile and 0.1% TFA for organic compound. The samples were prepared at a sample to matrix solution ratio of 1:4 (v/v) and 5 µl of the mixture deposited on the sample plate.

ICP-MS. The amount of platinum in conjugated samples and internalized in PANC-1 cancer cell lines, was determined by ICP-MS iCAP-Q (ThermoFisher) spectrometer. The samples were digested with aqua regia (overnight) and diluted with water before the measurements.

LC-MS. LC (Liquid chromatography) mass spectrometry was carried out using a UHPLC chromatography system (Acquity UPLC, Waters, Milford, USA) coupled with an ESI-TOF mass spectrometer (LCT Premier XE, Waters, Milford, USA). The chromatographic separation was performed on an Acquity BEH reversed phase C18 column, using a mobile phase consisting of 100 mM ammonium formate in water (A) and acetonitrile (B). The gradient method was as follows: 0-1.5 min at 99% A, 1.5-6 min to 1% A, 6-8 min at 1% A, 8-8.5 min to 99% A, 8.5-10 min to 99%. The mass spectrometry detection was accomplished working in positive / W mode. The MS range acquired was between m/z 100-1000. The capillary and cone voltages were set at 1500 and 100V, respectively. Masslynx v4.1 software was used to analyze chromatograms and spectra (Waters, Milford, MA, USA). The use of ammonium formate as a buffer in the aqueous mobile phase enables the detection of platinum complexes as ammonium adducts. Similarly, the presence of platinum can be confirmed by comparing experimental isotopic distributions with calculated ones.

Gel electrophoresis. 15% SDS-PAGE electrophoresis gels were used to monitor the conjugation reaction. Low range protein was used as marker (LMW II) and the conjugated fractions were mixed with SDS loading buffer. The gel was first imaged using UV-light to monitor the fluorescence of the functionalized riboflavin and then stained with Coomassie Blue.

Cell culture experiments. PANC-1 pancreatic cancer cell line was obtained from the American Type Tissue Collection (ATCC) and cultured in DMEM/F-12 medium (without phenol red) supplemented with 10% fetal bovine serum (FBS) and 1% penicillin/streptomycin at 37 °C under 5% CO_2. Cells were passed at 70% of confluence.

Cell viability was measured using resazurin assay. For the measurements, PANC-1 were seeded in 96-well plates with a density of 7500 cells per well and allowed to adhere overnight. The medium was then substituted with fresh complete medium containing the samples at the desired concentration and cells were incubated for another 24 hours. The medium was replaced by a solution mixture of DMEM/F-12 medium and resazurin, after a wash with 200 µl of DPBS, and the cells incubated at 37 °C for 3 hours. Viability measurements were then conducted at 37 °C. The samples were excited at 560 nm and the fluorescence collected at 590 nm. Fluorescence spectra were recorded with Biotek Synergy H1 microplate reader using sterilized Nuclon Delta Surface 96 well (Thermo Fisher Scientific). Cell viability was expressed as percent value calculated as:

$$\text{Cell viability (\%)} = 100 - (F.I._T / F.I._C * 100)$$

Where $F.I._T$ is the fluorescence of treated cells and $F.I._C$ is the fluorescence of the untreated cells.

For the cell irradiation experiments, blue light (460 nm, 3.5 mW/cm^2) was used. Cells were seeded, incubated for 24 hours with samples and washed with 200 µl of DPBS before being irradiated for 45 min. It was alternated a time period of 10 min light on/off, 15 min for the last irradiation section. Cell viability was then measured with resazurin assay, as described before.

2. Synthesis and characterization

Synthesis of *N*-(3-(7,8-dimethyl-2,4-dioxo-10-((2*R*,3*R*,4*S*)-2,3,4,5-tetrahydroxypentyl)-4,10-dihydrobenzo[*g*]pteridin-3(2*H*)-yl)propyl)-2-iodoacetamide (Rf-IA)

The iodoacetamide-functionalized riboflavin was prepared following the procedure described in Fig. S1. Previously reported methods were followed for the preparation of compounds I[2], II[3], and III.[4]

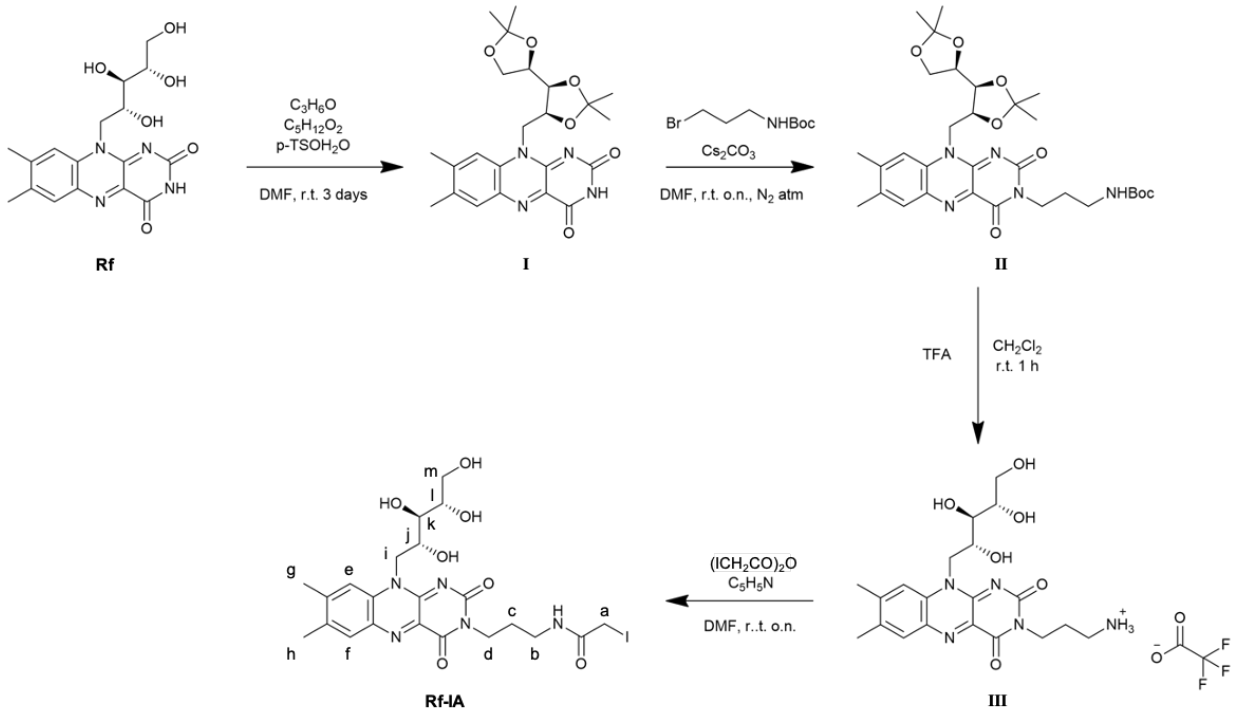

Fig. S1 Synthetic procedure adopted for the preparation of **Rf-IA**.

Step 1. 7,8-dimethyl-10-(((4*S*,4'*R*)-2,2,2',2'-tetramethyl-[4,4'-bi(1,3-dioxolan)]-5-yl)methyl)benzo[*g*]pteridine-2,4(3*H*,10*H*)-dione (I)

The starting point of our procedure was the protection of the hydroxyl groups of the ribityl chain by dimethyl acetal groups.[2] Commercial riboflavin (3 g) was dissolved in acetone (32 mL), dimethylformamide (40 mL), dimethoxypropane (16 mL) and p-toluenesulfonic acid monohydrate (1.5 g) was added. The resulting mixture was stirred at room temperature for 3 days. 80 mL of water were then added and the aqueous phase was extracted with CH_2Cl_2. The combined organic phases were dried over $MgSO_4$ and concentrated in vacuum. The product was then purified by centrifugation at 3500 rpm to remove DMF (after adding 3 mL of diethyl ether to the product) (2.5 g, 70%).

^{1}H-NMR (300 MHz, $CDCl_3$), δ(ppm): 8.05 (s, 1H, $H_{(f)}$), 7.65 (s, 1H, $H_{(e)}$), 5.23-3.97 (m, 7H, $H_{(i)}$, $H_{(j)}$, $H_{(k)}$, $H_{(l)}$, $H_{(m)}$), 2.53 (s, 3H, $H_{(h)}$), 2.46 (s, 3H, $H_{(g)}$), 1.52-1.20 (m, 12H, $C(CH_3)_2$) (* solvent impurities: 1.60 water).

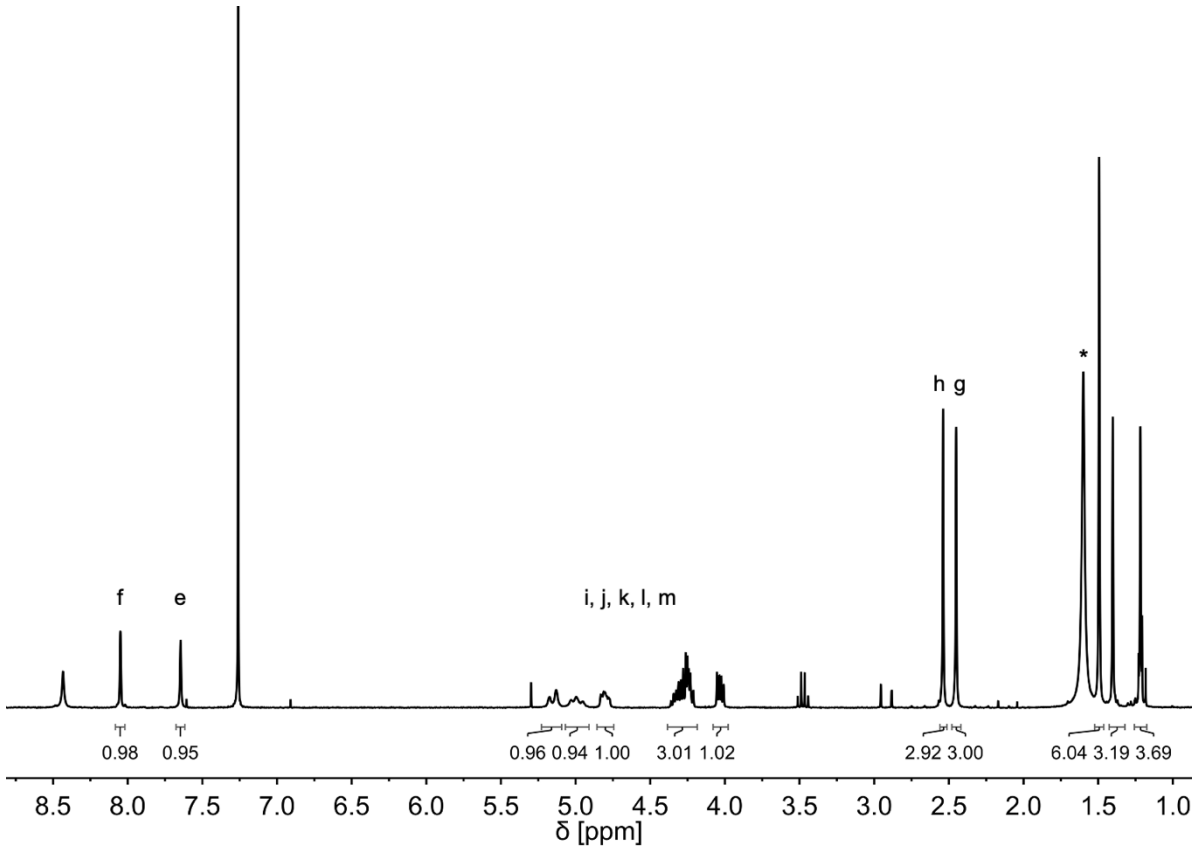

Step 2. Tert-butyl (3-(7,8-dimethyl-2,4-dioxo-10-(((4S,4'R,5S)-2,2,2',2'-tetramethyl-[4,4'-bi(1,3-dioxolan)]-5-yl)methyl)-4,10-dihydrobenzo[g]pteridin-3(2H)-yl)propyl)carbamate (II)

Subsequently, a nucleophilic substitution to the isoalloxazine N3 was performed.[3] The protected riboflavin (**I**) (0.470 g) and Cs_2CO_3 (0.505 g) were suspended in dry dimethylformamide (5 mL) and stirred under nitrogen for 30 min. Next, 3-(Boc-amino)propyl bromide was dissolved in 3 mL of dry DMF and added to the reaction mixture, which was left stirring overnight at room temperature under nitrogen. Afterwards, the mixture was portioned in CH_2Cl_2 and brine (saturated solution of NaCl) and the organic phase was washed with brine. The organic phase was kept, washed with $MgSO_4$, filtered and removed under vacuum. The brown oil obtained was purified by column chromatography (eluent CH_2Cl_2:MeOH 99:1) (0.47 g, 85%).

^{1}H-NMR (300 MHz, $CDCl_3$), δ(ppm): 8.01 (s, H, $H_{(f)}$), 7.62 (s, 1H, $H_{(e)}$), 5.20-3.98 (m, 9H, $H_{(i)}$, $H_{(j)}$, $H_{(k)}$, $H_{(l)}$, $H_{(m)}$, $H_{(d)}$), 2.53 (s, 3H, $H_{(h)}$), 2.45 (s, 3H, $H_{(g)}$), 1.91(p, 2H, J = 6.1 Hz, $H_{(c)}$), 1.52-1.17 (m, 21H, $C(CH_3)_3$). The $H_{(b)}$ signal is covered by DMF peaks (* solvents impurities: 8.01, 2.95 and 2.87 dimethylformamide, 5.30 dichloromethane)).

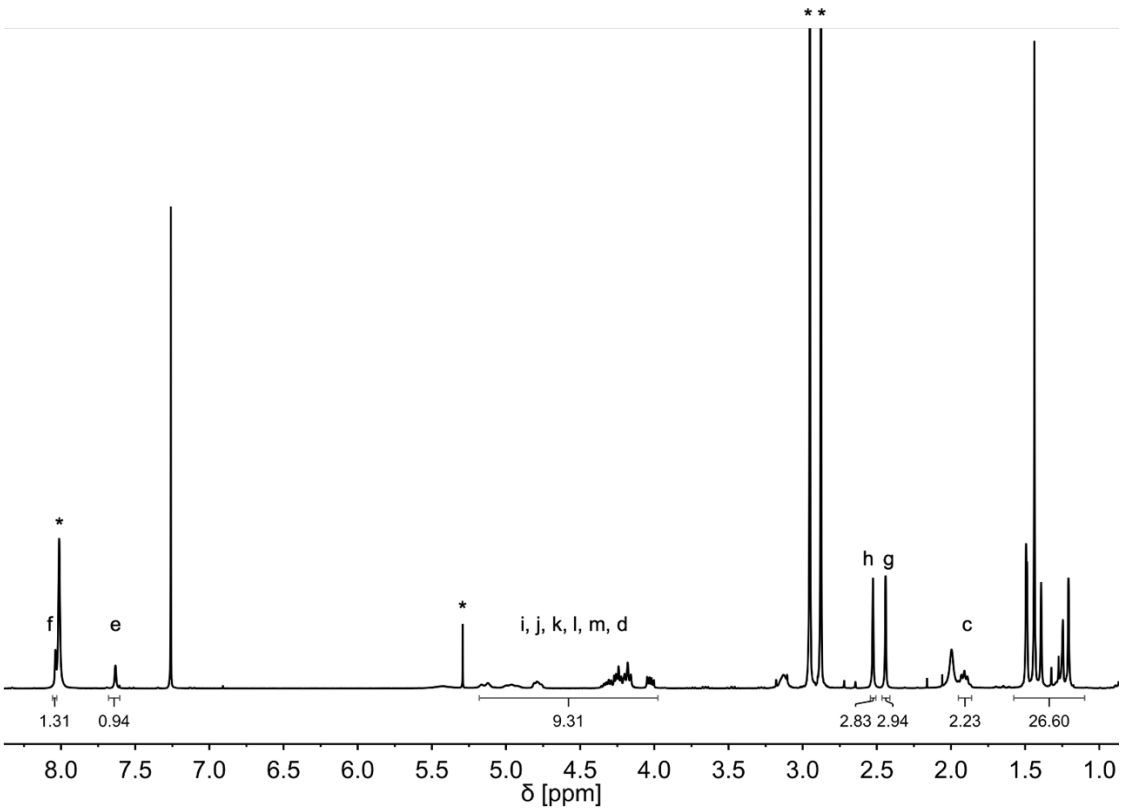

Step 3. 3-(7,8-dimethyl-2,4-dioxo-10-((2*R*,3*R*,4*S*)-2,3,4,5-tetrahydroxypentyl)-4,10-dihydrobenzo[*g*]pteridin-3(2*H*)-yl)propan-1-aminium (III)

Protecting groups were removed adapting a previously reported procedure.[4] The protected and functionalized riboflavin (0.160 g) was dissolved in 80 mL of CH_2Cl_2 in an ice bath under stirring. 3 mL of TFA were then added to the mixture and the ice bath was removed. The reaction was left stirring for 1 hour at room temperature. Then, the solvent was removed under vacuum and the product was washed four times with CH_2Cl_2. The final product was purified by column chromatography (eluent MeOH:H_2O 37:63) (0.066 g, 59 %).

^{1}H-NMR (300 MHz, CD_3OD), δ(ppm): 8.02 (s, 1H, $H_{(f)}$), 7.96 (s, 1H, $H_{(e)}$), 4.18 (t, 2H, J = 6.6 Hz, $H_{(d)}$), 3.91-3.64 (m, 5H, $H_{(i)}$, $H_{(j)}$, $H_{(k)}$, $H_{(l)}$, $H_{(m)}$), 3.00 (t, 1H, J = 7.2 Hz, $H_{(b)}$), 2.6 (s, 3H, $H_{(h)}$), 2.49 (s, 3H, $H_{(g)}$), 2.08 (p, 2H, J = 6.9 Hz, $H_{(c)}$) (* solvent impurities: 5.49 dichloromethane). ESI-MS, m/z $[M+H]^+$ calculated for $C_{21}H_{29}N_4O_6$: 433.21, found 434.5.

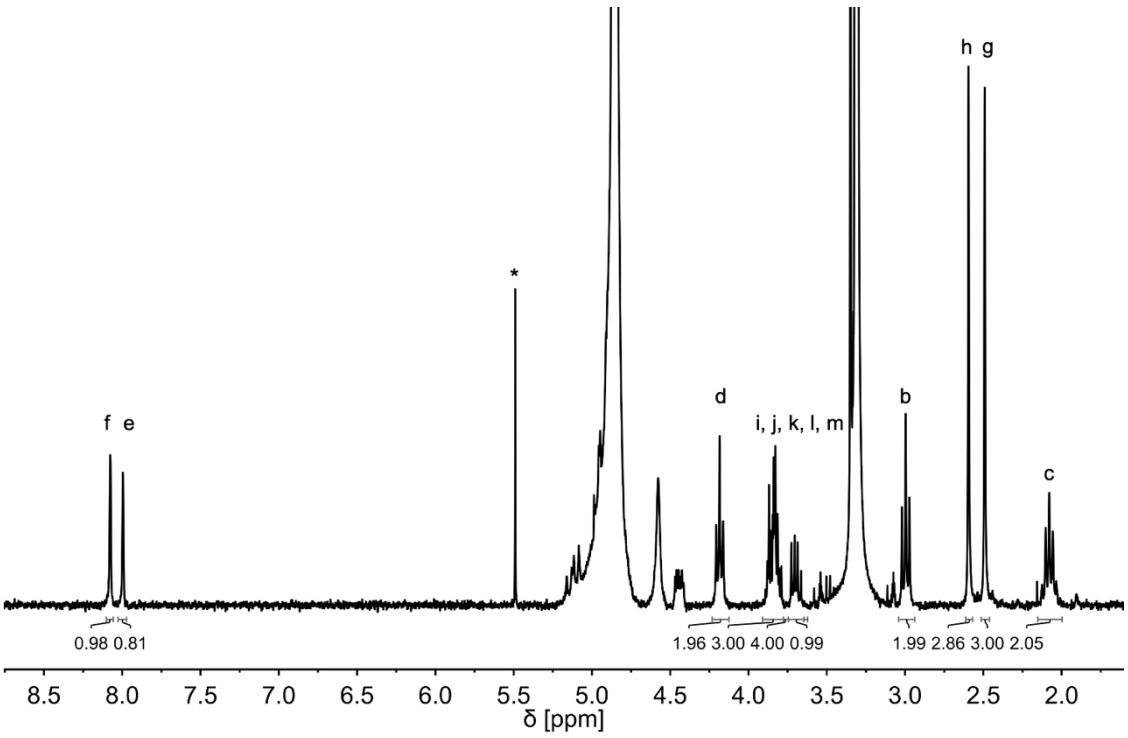

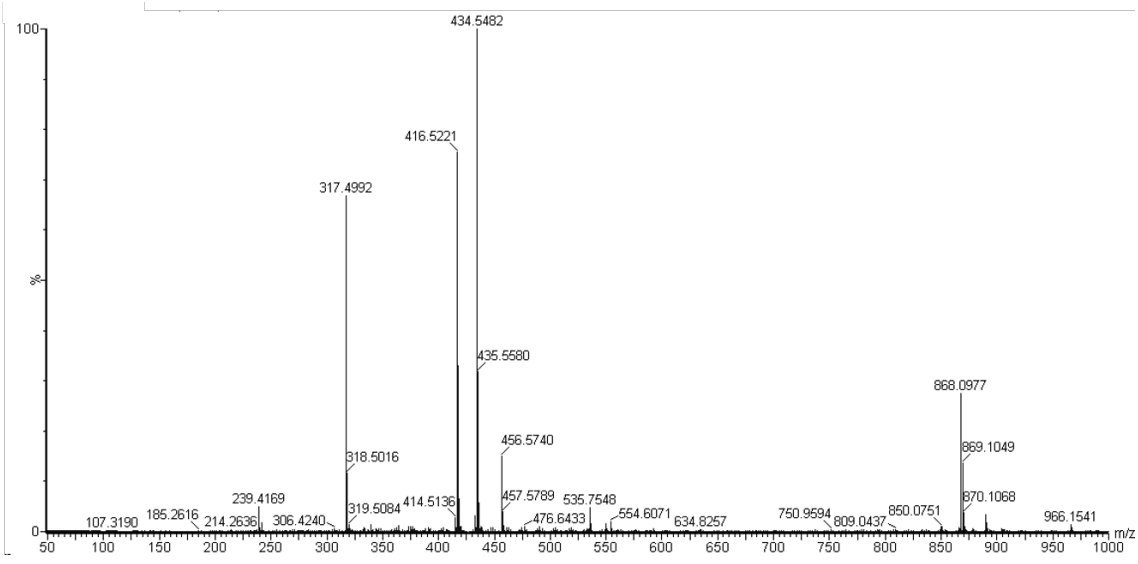

Step 4. *N*-(3-(7,8-dimethyl-2,4-dioxo-10-((2*R*,3*R*,4*S*)-2,3,4,5-tetrahydroxypentyl)-4,10-dihydrobenzo[*g*]pteridin-3(2*H*)-yl)propyl)-2-iodoacetamide (Rf-IA)

Functionalization of riboflavin with a terminal iodoacetamido group was achieved by reacting **III** with iodoacetic anhydride.[5]Iodoacetic anhydride (26.00 mg) dissolved in 5 mL of dry DMF was added dropwise to a solution (5 mL, dry DMF) of the riboflavin derivative **III** (45.10 mg). This reaction step was performed in an ice bath, which we removed at the end of the addition. Afterwards, the reaction was left stirring overnight. The solvent was removed under vacuum and **Rf-IA** was subsequently purified by column chromatography (eluent MeOH:CH_2Cl_2 from 1:5 to MeOH:CH_2Cl_2 1:3) (6.4 mg, 15%).

^{1}H-NMR (300 MHz, CD_3OD), δ(ppm): 8.06 (s, 1H, $H_{(f)}$), 4.13 (t, 2H, J = 6.9 Hz, $H_{(d)}$), 3.91-3.61 (m, 7H, $H_{(i)}$, $H_{(j)}$, $H_{(k)}$, $H_{(l)}$, $H_{(m)}$), 3.71 (s, 2H, $H_{(a)}$), 2.58 (s, 3H, $H_{(h)}$), 2.47 (s, 3H, $H_{(g)}$), 1.93 (p, 2H, J = 6.9 Hz, $H_{(c)}$). The $H_{(e)}$, $H_{(b)}$ signals are covered by DMF peaks (* solvent impurities: 7.95 dimethylformamide). $^{13}C\{^1H\}$ (125.7 MHz, CD_3OD), δ(ppm): 132.13 (1C, $C_{(e)}$), 131.66 (1C, $C_{(f)}$), 127.49 (1C, **C**CN), 124.86 (1C, NC**C**N), 75.22-71.20 (3C, $C_{(j)}$, $C_{(k)}$, $C_{(l)}$), 64.79 (1C, $C_{(m)}$), 40.60-38.75 (2C, $C_{(i)}$, $C_{(d)}$), 28.48 (1C, $C_{(c)}$), 21.40-19.40 (2C, **C**(CH_3)C, C(CH_3)**C**), -2.70 (1C, $C_{(a)}$). ESI-MS, m/z $[M+H]^+$ calculated for $C_{22}H_{28}IN_5O_7$: 600.11, found 600.

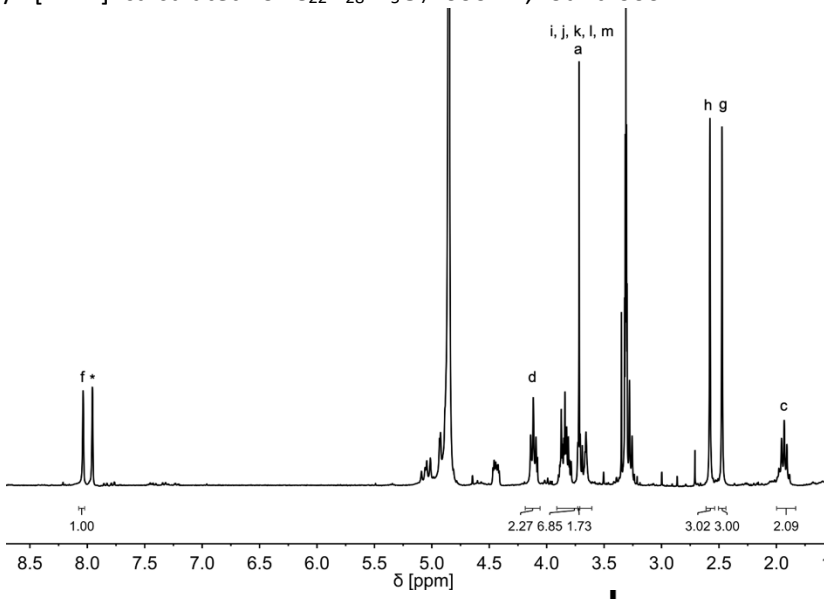

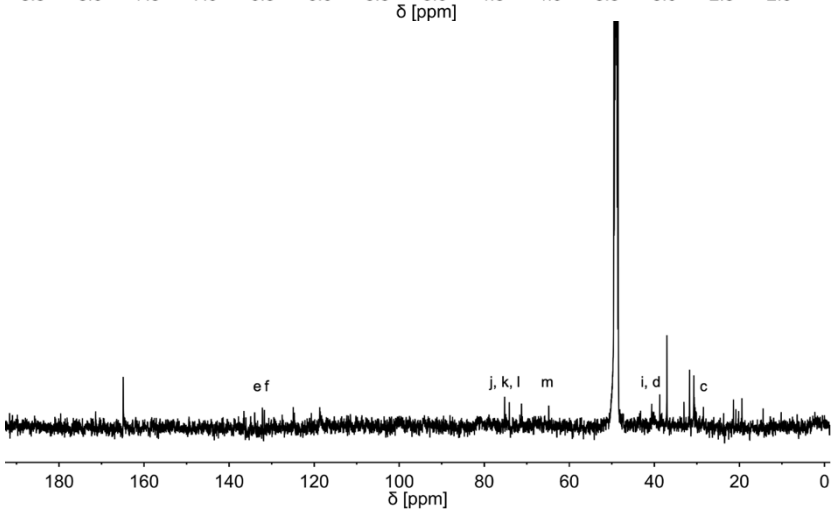

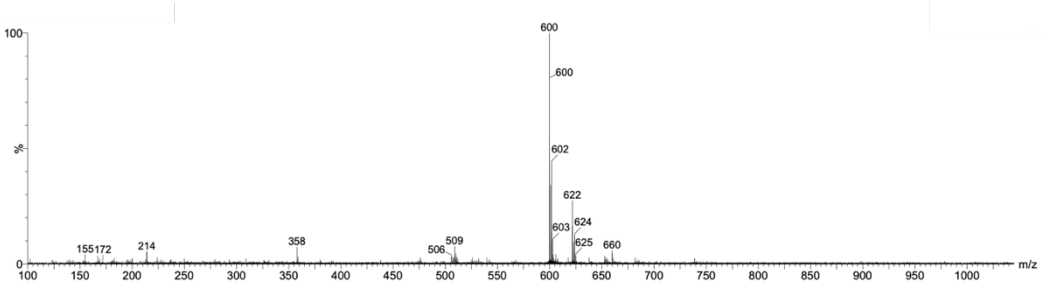

Synthesis of *cis,cis,trans*-[Pt(NH$_3$)$_2$(Cl)$_2$(OCOCH$_3$)(O$_2$CCH$_2$CH$_2$CO$_2$H)] (Pt1) and its NHS-activated derivative (Pt1-NHS)

The **Pt1** complex was prepared following the procedure described in Fig. S2. Previously reported methods were adopted for the preparation of cisplatin[6,7], IV[8], **Pt1**[8] and **Pt1-NHS.**[8]

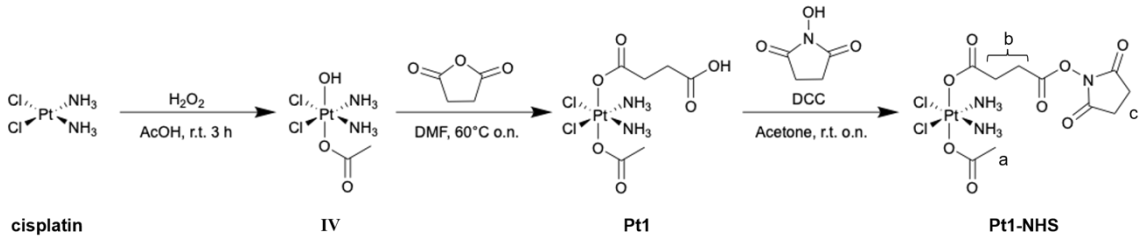

Fig. S2 Synthetic procedure for the preparation of **Pt1** and **Pt1-NHS**.

Step 1. cis-diamminedichloroplatinum(II) (*cisplatin*)

Cisplatin was prepared following the procedure reported by Smith and co-workers.[7]

Step 2. *cis,cis,trans*-[Pt(NH$_3$)$_2$(Cl)$_2$(OH)(OCOCH$_3$)] (IV)

0.20 g of cisplatin were suspended in 97 mL of acetic acid, then 2 mL of hydrogen peroxide were added. The mixture was left stirring at room temperature for 3 hours, protected by light. Progressively, the solution became clear. Next, the reaction mixture was centrifuged (6000 rpm, 3 min) to remove unreacted cisplatin. The supernatant was concentrated under reduced pressure.

An excess of diethyl ether was added to the residue to favor the precipitation of a yellow solid. The product was collected by centrifugation and washed with acetone, dichloromethane, and ether. The final product, **IV,** was characterized by ^{1}H-NMR, confirming previously reported assignments.[8]

^{1}H-NMR (300 MHz, (CD$_3$)$_2$SO), δ(ppm): 6.25-5.70 (m, 6H, 2NH$_3$), 1.87 (s, 3H, H$_{(a)}$) (* solvents impurities: 5.75 dichloromethane, 3.33 water, 2.09 acetone, 1.91 acetic acid).

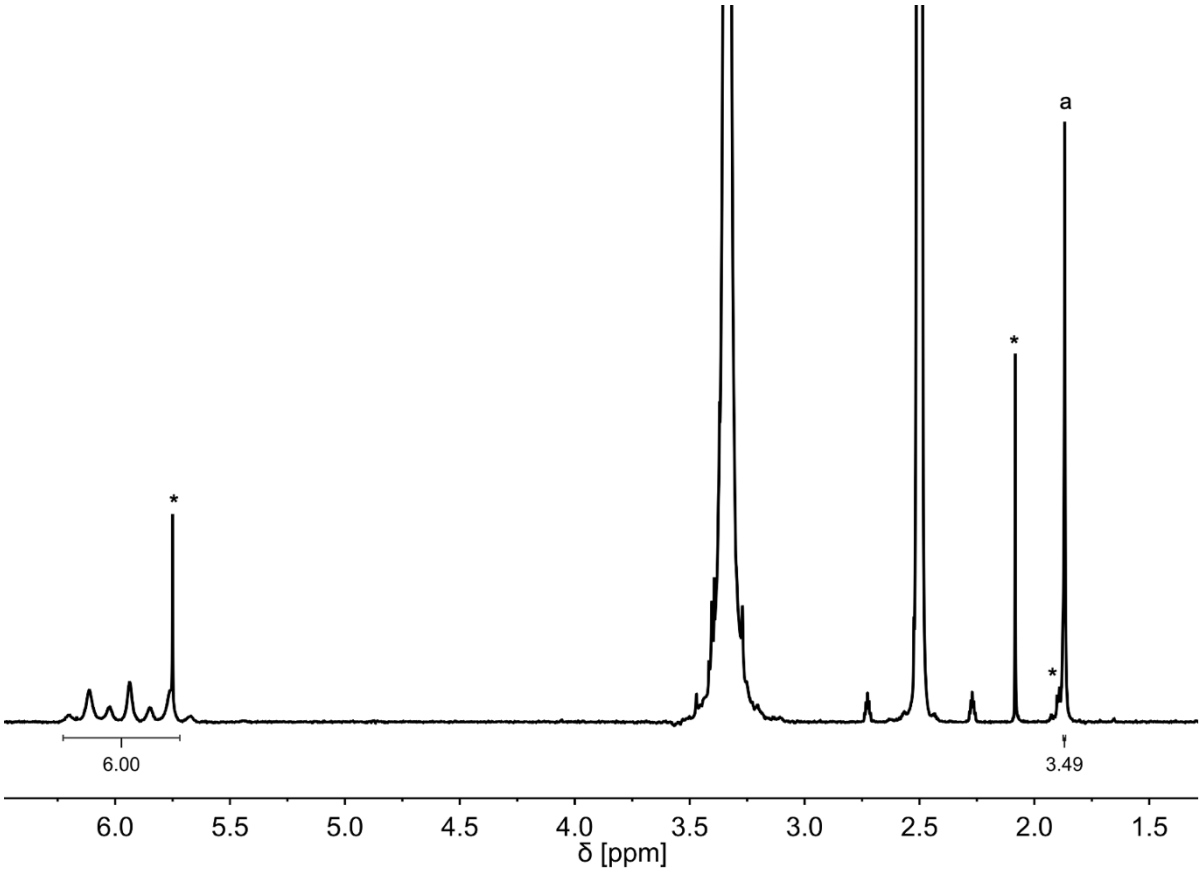

Step 3. ***cis,cis,trans*-[Pt(NH$_3$)$_2$(Cl)$_2$(OCOCH$_3$)(O$_2$CCH$_2$CH$_2$CO$_2$H)] (Pt1)**

0.16 g of **IV** were suspended in 1 mL of dry DMF. Succinic anhydride, 0.25 g (6 eq), was then added. The mixture was stirred at 60°C overnight, protected by light.

The day after, 1.5 mL of CH_2Cl_2 and 45 mL of diethyl ether were added to the reaction mixture to form a yellow solid. The mixture was centrifuged (6500 rpm, 3 min) and was dissolved three times with 1mL of CH_2Cl_2 and 15 mL of diethyl ether. Before the addition of diethyl ether, the product was sonicated until all the product was in suspension. The final product, **Pt1,** was characterized by NMR and ESI-MS as previously reported.[8]

^{1}H-NMR (300 MHz, $(CD_3)_2SO$), δ(ppm): 2.42-2.29 (m, 4H, $H_{(b)}$), 1.90 (s, 3H, $H_{(a)}$) (* solvents impurities: 2.89 and 2.73 dimethylformamide, 1.91 acetic acid). ESI-MS: m/z $[M+H]^+$ calculated for $C_6H_{13}Cl_2N_2O_6Pt$: 475.98, found 476.86

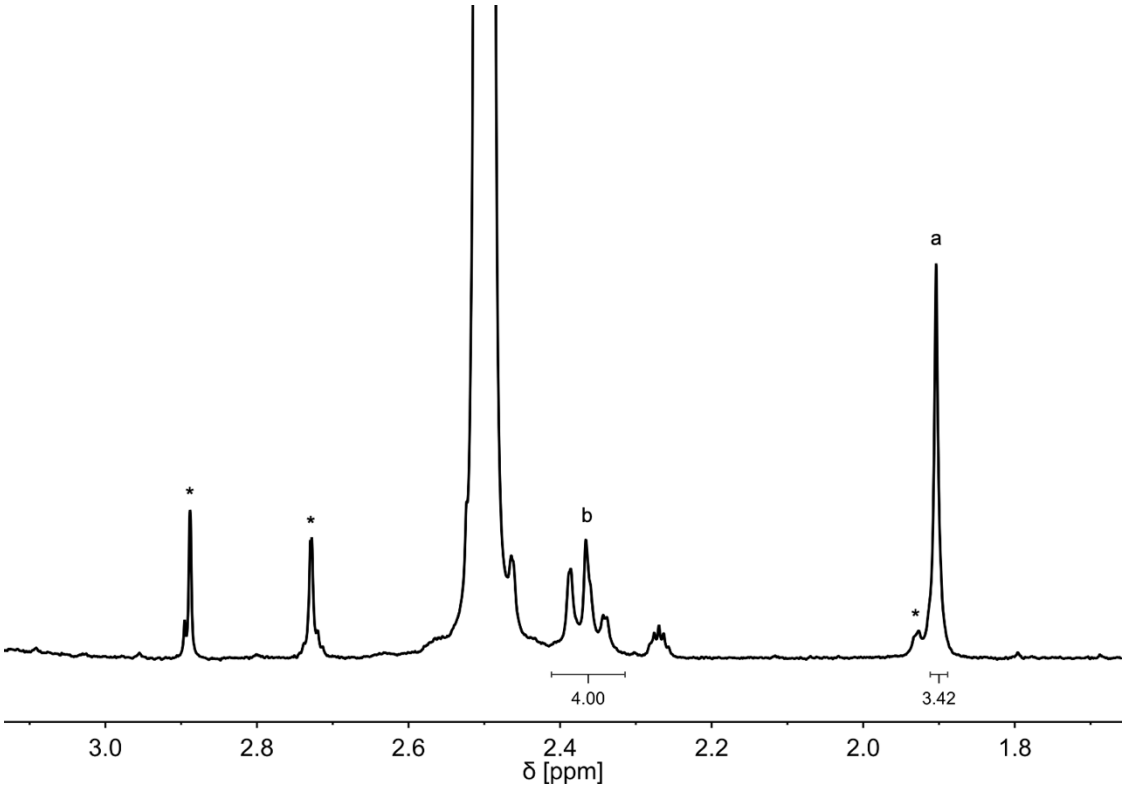

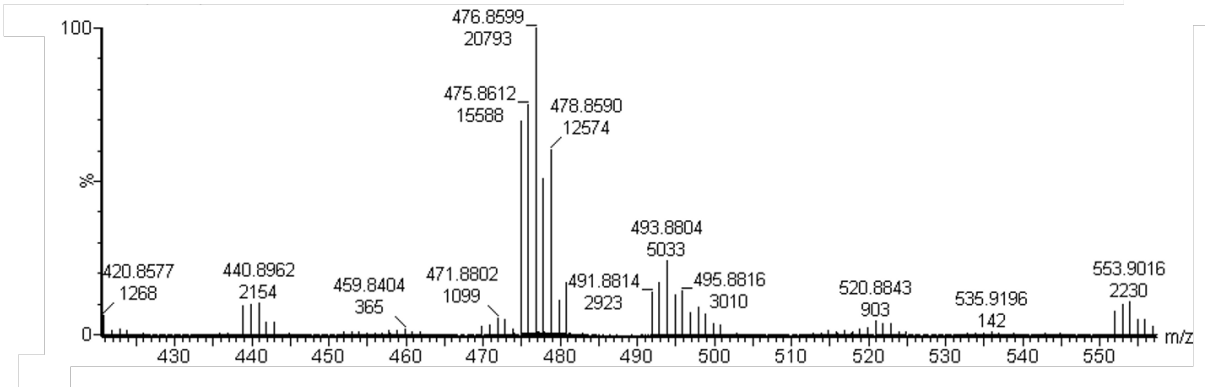

Step 4. Synthesis of N-Hydroxysuccinimide-Activated *cis,cis,trans*-[Pt(NH$_3$)$_2$(Cl)$_2$(OCOCH$_3$)(O$_2$CCH$_2$CH$_2$CO$_2$H)] (Pt1-NHS)

134 mg of **Pt1** were dissolved in 8 mL of anhydrous acetone. Subsequently, 48.58 mg (1.50 eq) of N-hydroxysuccinimide (NHS) and 70 mg of N,N'-dicyclohexylcarbodiimide (DCC) were added to the mixture which was left stirring overnight at room temperature, protected by light.

The solution was cooled for 1 hour in the freezer and the precipitate was removed by filtration. The product was washed by partial dissolution in acetone (1-2 mL), sonicated and precipitated with diethyl ether (10 mL) four times. The final product, **Pt1-NHS,** was characterized by NMR and ESI-MS confirming literature data.[8]

^{1}H-NMR (300 MHz, (CD$_3$)$_2$SO), δ(ppm): 2.85-2.60 (m, 8H, H$_{(b)}$, H$_{(c)}$), 1.90 (s, 3H, H$_{(a)}$). ESI-MS, m/z [M+H]$^+$ calculated for $C_{10}H_{17}Cl_2N_3O_8Pt$: 573.00, found 573.84.

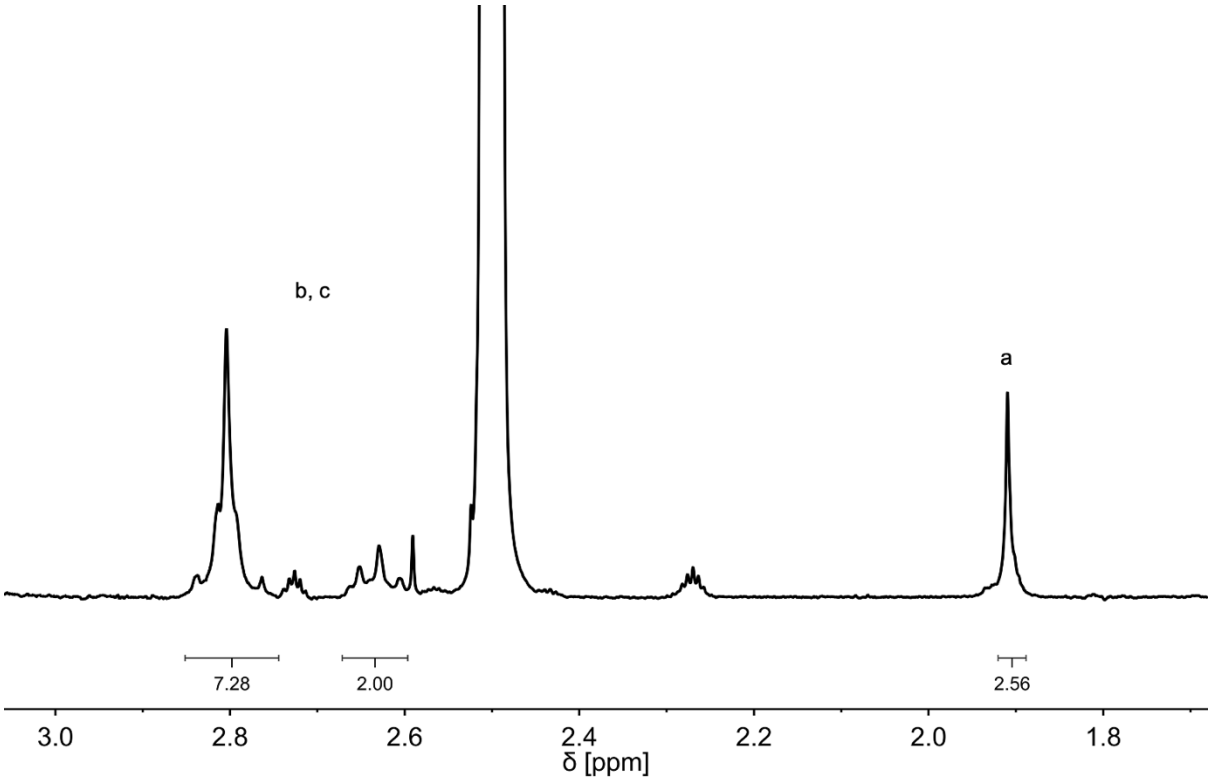

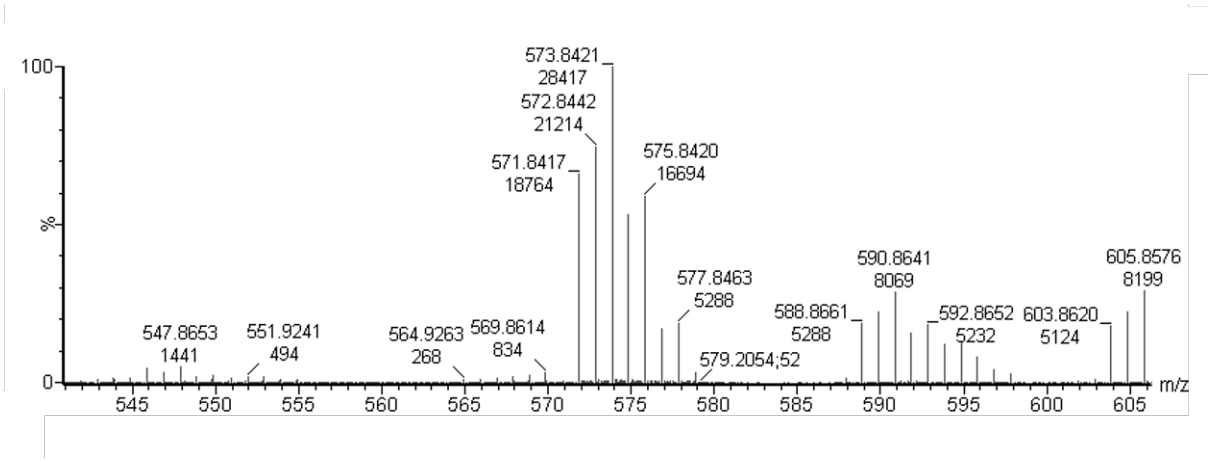

Synthesis of *cis,cis,trans*-[Pt(NH$_3$)$_2$(Cl)$_2$(O$_2$CCH$_2$CH$_2$CO$_2$H)$_2$] (Pt2)

The Pt2 complex was prepared following the procedure described in Fig. S3. Previously reported methods were adopted for the preparation of cisplatin[6,7], **V**[9] and **Pt2**.[9]

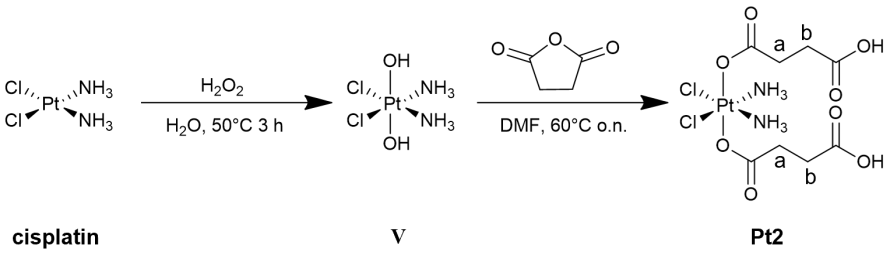

Fig. S3 Synthetic procedure for the preparation of **Pt2**.

Step 1. *cis,cis,trans*-[Pt(NH$_3$)$_2$(Cl)$_2$(OH)$_2$] (V)

0.18 g of cisplatin were suspended in 1.5 mL of water and then 9 mL of hydrogen peroxide were added. The mixture was left stirring at 50°C for 3 hours, protected by light. Progressively, the solution became clear. Next, the reaction mixture was centrifuged (6000 rpm, 3 min) to remove unreacted cisplatin. The supernatant was concentrated under reduced pressure.

An excess of diethyl ether was added to the residue to favor the precipitation of a yellow solid. The product was collected by centrifugation and washed with acetone, dichloromethane and ether. The final product, **V**, was characterized by ^{1}H-NMR, confirming previously reported assignments.[9]

^{1}H-NMR (300 MHz, (CD$_3$)$_2$SO), δ(ppm): 10.2 (s, H$_{(NH3)}$).

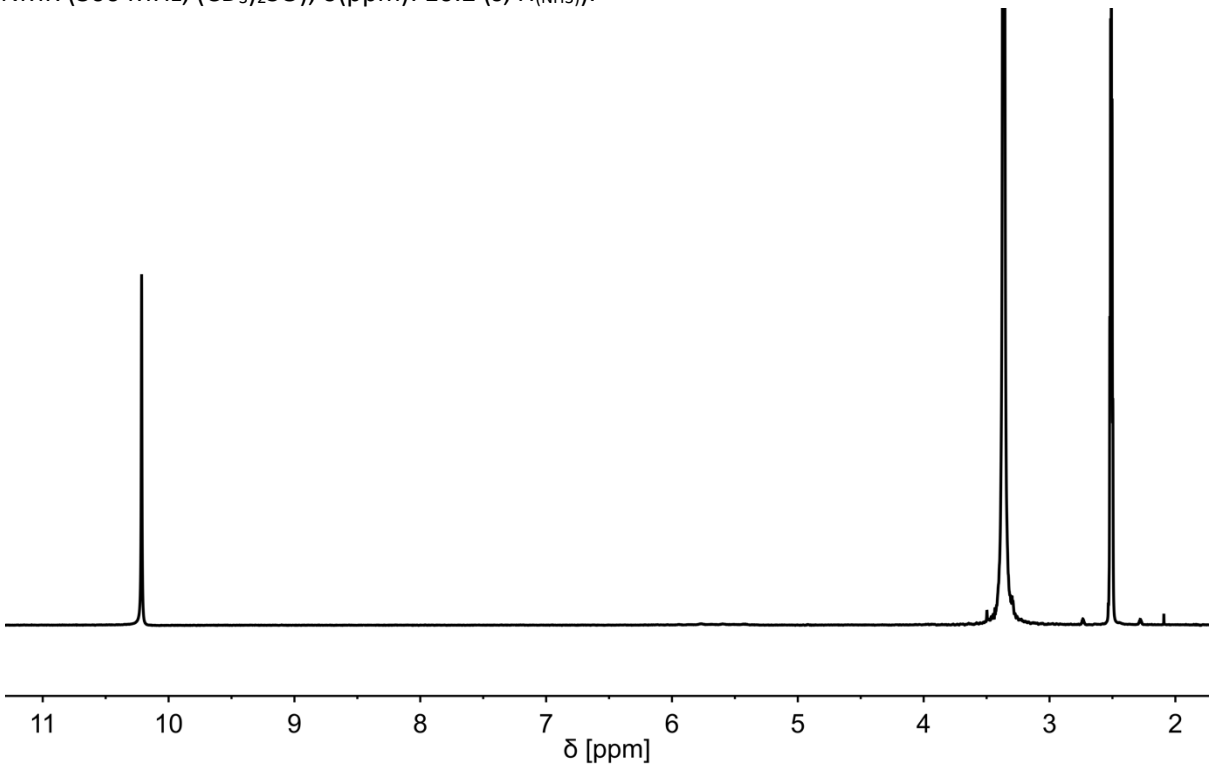

Step 2. *cis,cis,trans*-[Pt(NH$_3$)$_2$(Cl)$_2$(O$_2$CCH$_2$CH$_2$CO$_2$H)$_2$] (Pt2)

96.4 mg of **V** were suspended in 1 mL of dry DMF. Succinic anhydride, 115.7 mg (4 eq.), was then added. The mixture was stirred at 60°C overnight, protected by light.

The day after, 1.5 mL of CH_2Cl_2 and 45 mL of diethyl ether were added to the reaction mixture to form a yellow solid. The mixture was centrifuged (6500 rpm, 3 min) and was dissolved three times with 1mL of CH_2Cl_2 and 15 mL of diethyl ether. Before the addition of diethyl ether, the product was sonicated until all the

product was in suspension. The final product, **Pt2**, was characterized by NMR and ESI-MS as previously reported.[9]

^{1}H-NMR (300 MHz, D_2O), δ(ppm): 2.56 (t, J = 6.9 Hz, $H_{(b)}$), 2.33 (t, J = 7.0 Hz, $H_{(a)}$) (* solvents impurities: 3.56 diethyl ether, 2.94 and 2.80 dimethylformamide, 2.16 acetone). ESI-MS: m/z $[M+H]^+$ calculated for $C_8H_{16}Cl_2N_2O_8Pt$: 534, found 535.43.

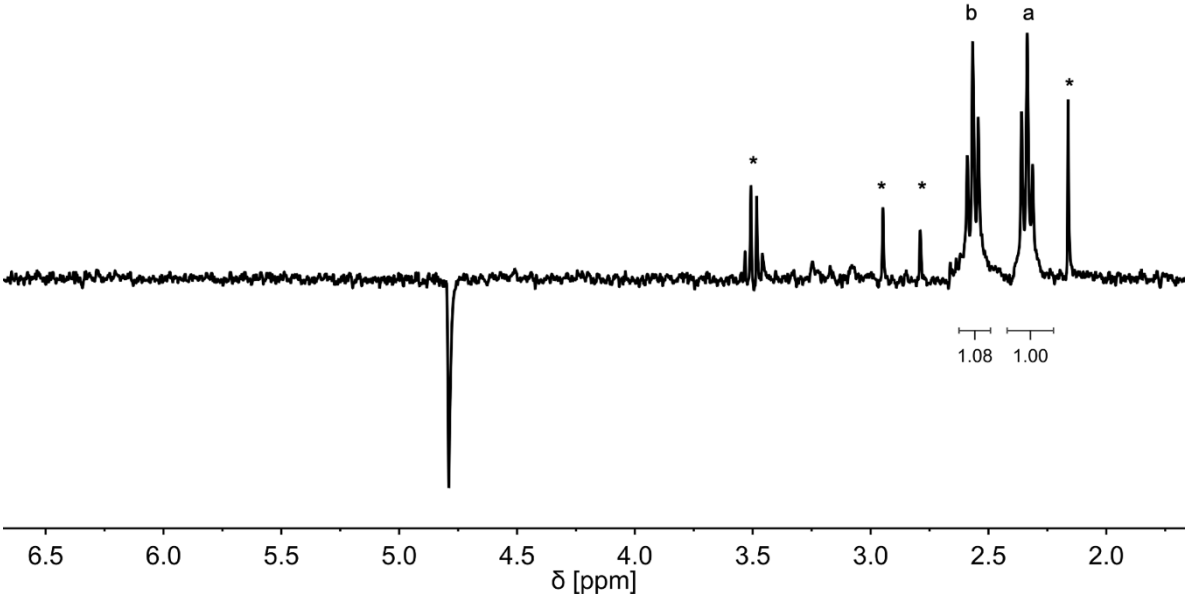

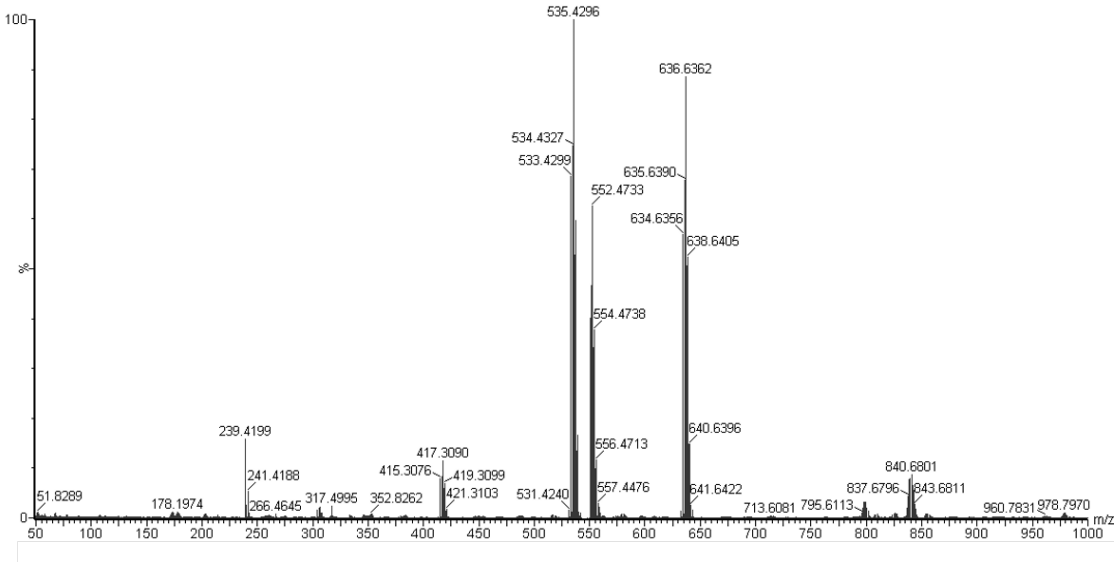

3. Protein design and purification

CTPR4/CTPR6/CTPR8. Based on a consensus CTPR4 protein cloned into pPro-EXHTa, two cysteine residues were introduced at positions 17 in the first and third CTPR repeat. The CTPR4 obtained is composed by alternating modules without any mutation, called wild type module (WT, (A E A W Y N L G N A Y Y K Q G D Y D E A I E Y Y Q K A L E L D P R S), as second and fourth ones, and with two cysteine modules, as first and third ones. The expressed proteins present some additional residues at the N-terminus derived from the cloning strategy and a solvating helix at the C-terminus. The sequence of the amino acids for CTPR4 is reported below. The two cysteines mutation positions are underlined in blue, the His-tag in green and the solvating helix in purple:

CTPR4

M S Y Y H H H H H H D Y D I P T T E N L Y F Q G A M G S
A E A W H N L G H A Y Y K Q G D **C** D E A I E Y Y Q K A L E L D P R S
A E A W Y N L G N A Y Y K Q G D Y D E A I E Y Y Q K A L E L D P R S
A E A W H N L G H A Y Y K Q G D **C** D E A I E Y Y Q K A L E L D P R S
A E A W Y N L G N A Y Y K Q G D Y D E A I E Y Y Q K A L E L D P R S
A E A K Q N L G N A K Q K Q G

Based on the mutated CTPR4, previously reported, two and four CTPR(WT) repeats were added to obtain CTPR6 and CTPR8, respectively. The sequences of the amino acids are reported below for CTPR6 and CTPR8, respectively. The two cysteines mutation positions are underlined ion blue, the His-tag in green and the solvating helix in purple:

CTPR6

M S Y Y H H H H H H D Y D I P T T E N L Y F Q G A M G S
A E A W H N L G H A Y Y K Q G D **C** D E A I E Y Y Q K A L E L D P R S
A E A W Y N L G N A Y Y K Q G D Y D E A I E Y Y Q K A L E L D P R S
A E A W H N L G H A Y Y K Q G D **C** D E A I E Y Y Q K A L E L D P R S
A E A W Y N L G N A Y Y K Q G D Y D E A I E Y Y Q K A L E L D P R S
A E A W Y N L G N A Y Y K Q G D Y D E A I E Y Y Q K A L E L D P R S
A E A W Y N L G N A Y Y K Q G D Y D E A I E Y Y Q K A L E L D P R S
A E A K Q N L G N A K Q K Q G

CTPR8

M S Y Y H H H H H H D Y D I P T T E N L Y F Q G A M G S
A E A W H N L G H A Y Y K Q G D **C** D E A I E Y Y Q K A L E L D P R S
A E A W Y N L G N A Y Y K Q G D Y D E A I E Y Y Q K A L E L D P R S
A E A W H N L G H A Y Y K Q G D **C** D E A I E Y Y Q K A L E L D P R S
A E A W Y N L G N A Y Y K Q G D Y D E A I E Y Y Q K A L E L D P R S
A E A W Y N L G N A Y Y K Q G D Y D E A I E Y Y Q K A L E L D P R S
A E A W Y N L G N A Y Y K Q G D Y D E A I E Y Y Q K A L E L D P R S
A E A W Y N L G N A Y Y K Q G D Y D E A I E Y Y Q K A L E L D P R S
A E A W Y N L G N A Y Y K Q G D Y D E A I E Y Y Q K A L E L D P R S
A E A K Q N L G N A K Q K Q G

All the proteins were expressed as His-tagged fusion and purified first using standard affinity chromatography methods based on previously published protocols[10] for His-tagged CTPR proteins using 0.5% deoxycholic acid in the lysis buffer and secondly by size exclusion chromatography through a HiLoad 16/600 Superdex 75 pg (for CTPR4 and CTPR6) and HiLoad 16/600 Superdex 200 pg (for CTPR8) column using FPLC. The proteins were

then stored in PBS buffer (140 mM NaCl, 50 mM phosphate buffer pH 7.4) with β-mercaptoethanol frozen at –20°C. The protein concentration was determined by UV-absorbance at 280 nm using the extinction coefficient calculated from the amino acid composition (ε_{CTPR4} = 54905 M^{-1} cm^{-1}, ε_{CTPR6} = 83660 M^{-1} cm^{-1}, ε_{CTPR8} = 114030 M^{-1} cm^{-1}).

4. Bioconjugation of CTPRs

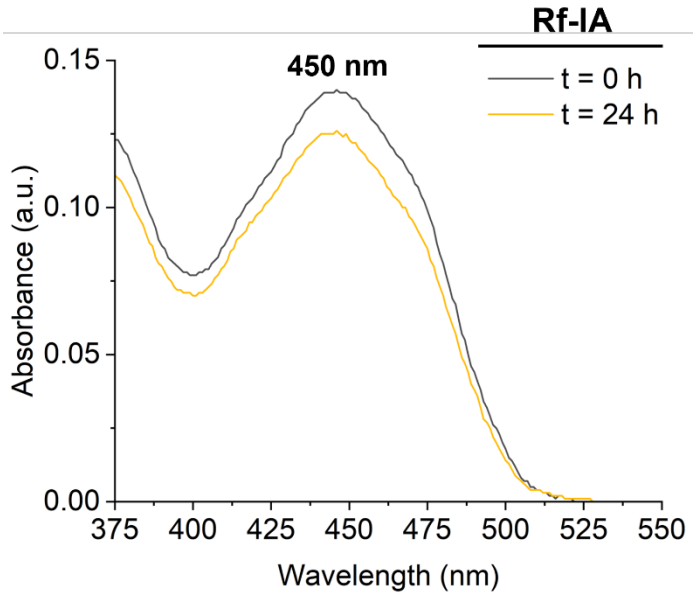

Fig. S4 UV-Vis spectra of **Rf-IA** molecule in PBS buffer (140 mM NaCl, 50 mM phosphate buffer pH 8.5), over 24 hours.

$CTPR_n$-Rf bioconjugation

We adopted the same procedure for the riboflavin bioconjugation of the three protein scaffolds, namely CTPR4, CTPR6 and CTPR8.[11]

Prior to any conjugation, purified CTPR at a protein concentration of about 100 µM was freshly reduced with 1 mM 1,4-dithio-DL-treitol (DTT) for 20 minutes to ensure full reduction of the cysteine residues. DTT was removed by buffer exchange over a Nap-5 column (GE Healthcare Life Science, prepacked with Sephadex G-25) in PBS buffer (140 mM NaCl, 50 mM phosphate buffer, pH 8.5). Protein fractions without DTT were eluted directly in the **Rf-IA** solution giving a ratio of 1:5.6 cysteine:**Rf-IA**. The coupling reaction occurred overnight, at room temperature and covered from light. The reaction mixture was then passed through a PD-10 desalting column (GE Healthcare Life Science, prepacked with Sephadex G-25) to eliminate the free dye. The final concentration of CTPR and functionalized riboflavin linked to the protein scaffold was calculated from the absorption spectra taking in account the absorbance correction for the protein's peak at 274 nm. The correction was calculated employing the following equation:

$$A_{274}(corr) = A_{274} - [A_{450}(dye) * CF_{274}(dye)]$$

$$CF_{274}(dye) = A_{274} / A_{450}$$

where A_{274} is the absorbance of the sample at 274 nm, $A_{450}(dye)$ is the absorbance at 450 nm of the functionalized riboflavin, $CF_{274}(dye)$ is the correction factor for the dye at 274 nm (Fig. S5).[12]

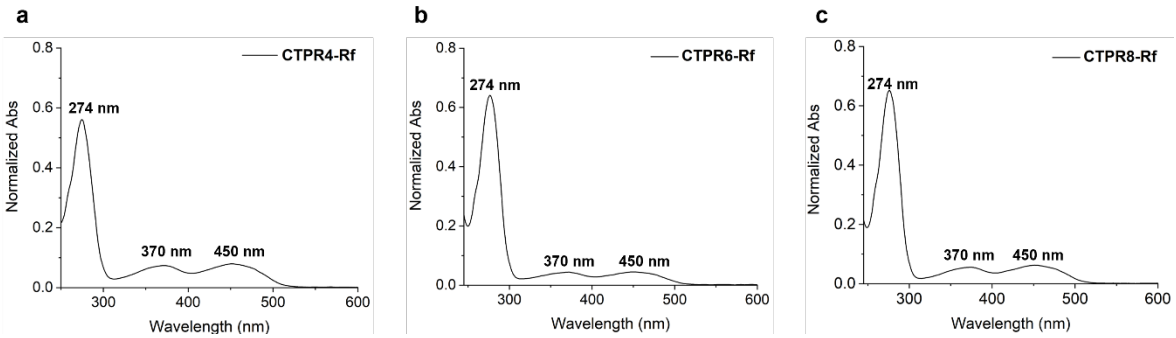

Fig. S5 UV-Vis spectra of conjugated systems: (a) **CTPR4-Rf**, (b) **CTPR6-Rf** and (c) **CTPR8-Rf** in PBS buffer (140 mM NaCl, 50 mM phosphate buffer pH 8.5) after the elimination of free functionalized riboflavin.

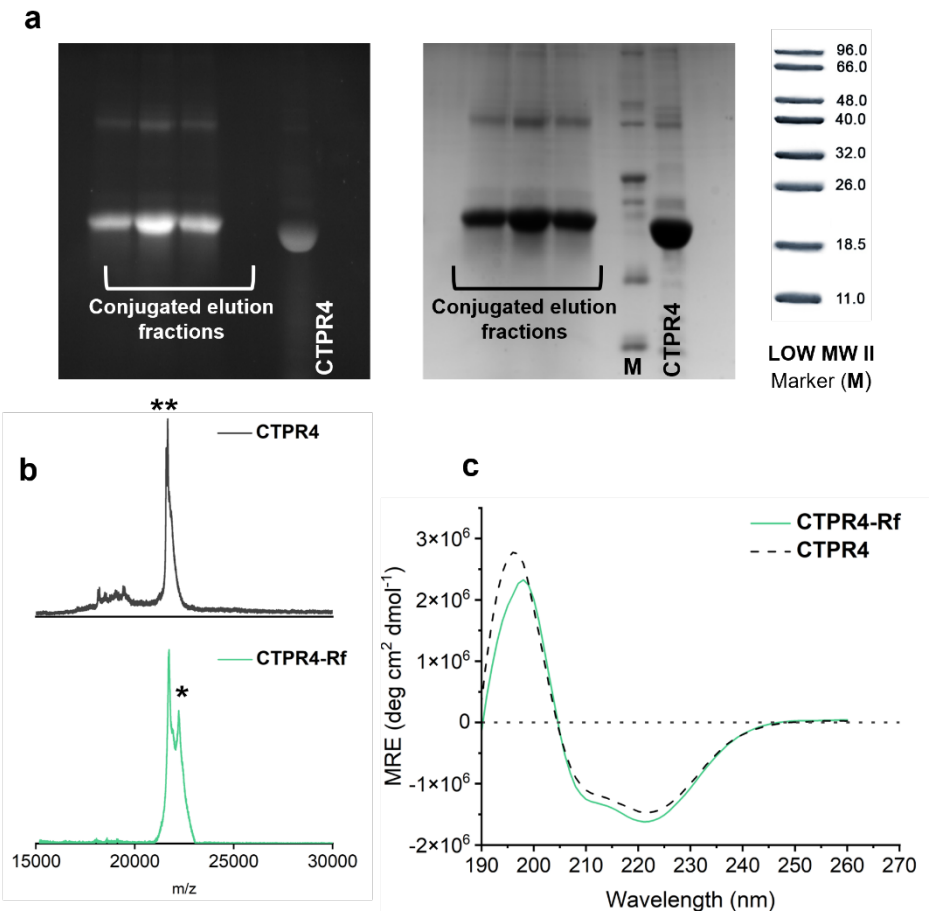

Fig. S6 Characterization of the **CTPR4-Rf** conjugate. (a) SDS-PAGE gels electrophoresis of **CTPR4-Rf** elution volumes, **CTPR4** and marker. The gel is imaged using UV light to monitor the fluorescence of riboflavin (left) and after Coomassie Blue staining (right). (b) MALDI-TOF spectra of **CTPR4-Rf** and **CTPR4** control. Peak assignment: 21.7 kDa **CTPR4**, 22.2 kDa **CTPR4** (21.66 kDa) + **Rf** (MW_{Rf} = 474 Da, molecular weight without the leaving group, I). (c) CD spectra in PB buffer of **CTPR4-Rf** (green) and **CTPR4** (black dashed) in the spectral region of the protein secondary structure absorption.

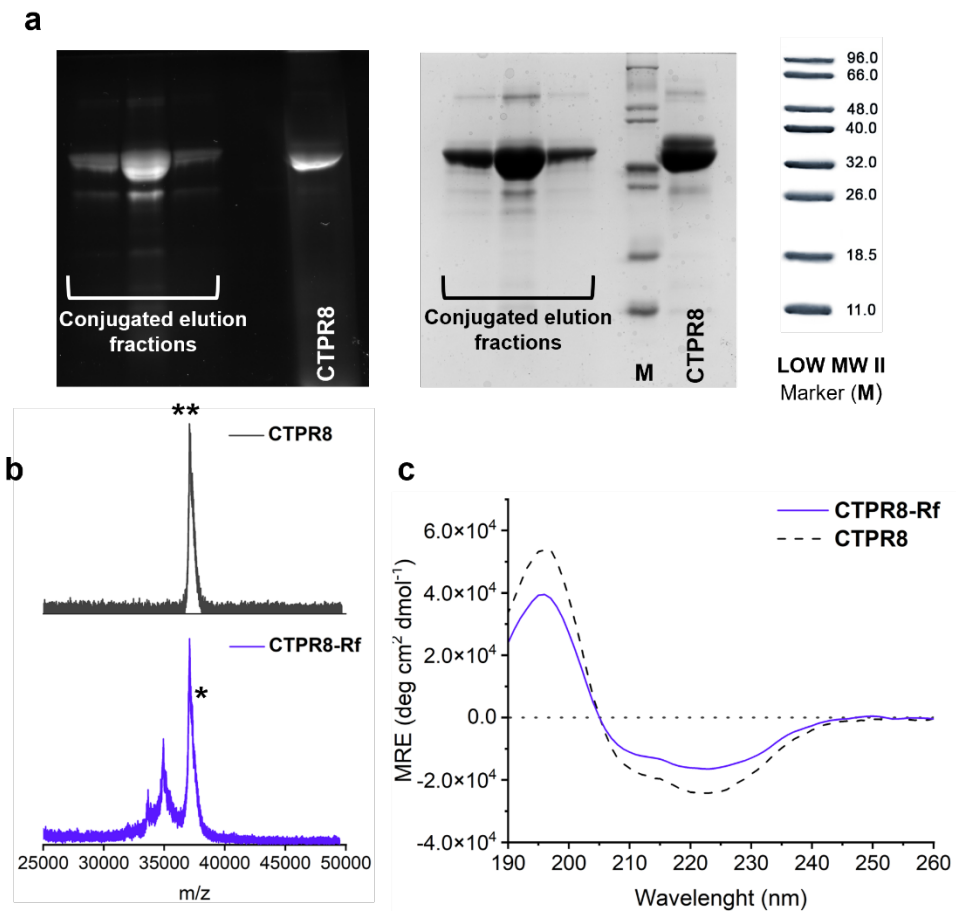

Fig. S7 Characterization of the **CTPR8-Rf** conjugate. (a) SDS-PAGE gels electrophoresis of the **CTPR8-Rf** conjugations elution volumes, CTPR8 alone and marker. The gel is imaged using UV light to monitor the fluorescence of riboflavin (left) and after Coomassie Blue staining (right). (c) MALDI-TOF spectra of **CTPR8-Rf** and **CTPR8** alone (control). Peak assignment: 37.0 kDa **CTPR8**, 37.4 kDa **CTPR8** (37.0 kDa) + **Rf** (MW_{Rf} = 474 Da, molecular weight without the leaving group, I). (d) CD spectra in PB buffer of **CTPR8-Rf** conjugate (purple) and CTPR alone (dash) in the spectral region of the protein secondary structure absorption.

CTPR6-Rf-Pt1 bioconjugation

CTPR6-Rf conjugated samples were reacted with the NHS-activated Pt complex (**Pt1-NHS**). To a 25 µM CTPR6(2Cys), 10 eq of **Pt1-NHS** (stock solution: 4.6 mM in PBS buffer 140 mM NaCl, 50 mM phosphate buffer, pH 7.4) were added using a lysine:Pt ratio of 1:10. The reaction was carried out overnight, at room temperature and covered from light. The reaction mixture was passed through a PD-10 desalting column (GE Healthcare Life Science, prepacked with Sephadex G-25) to eliminate unreacted **Pt1-NHS** complex. The final concentration of metal complex linked to CTPR6 scaffold was calculated with ICP-MS resulting in a ratio of 1:5 CTPR6:Pt. *Note:* conjugation reaction of 2 h should be optimal based on tests performed at a later stage monitoring the stability of **Pt1-NHS** in PBS buffer (pH 7.4) overtime.

CTPR6-Pt1 bioconjugation

To a 25 µM CTPR6, 10 eq of **Pt1-NHS** (stock solution: 4.6 mM in PBS buffer, 140 mM NaCl, 50 mM phosphate buffer, pH 7.4) were added using a lysine:Pt ratio of 1:10. The reaction occurred overnight, at room temperature and covered by light. The reaction mixture was passed through a PD-10 desalting column (GE Healthcare Life Science, prepacked with Sephadex G-25) to eliminate free **Pt1-NHS** complex. The final concentration of metal complex linked to the CTPR6 scaffold was calculated by ICP-MS mass spectrometry measurements resulting in a ratio of 1:5 CTPR6:Pt. *Note:* conjugation reaction of 2 h should be optimal based on tests performed at a later stage monitoring the stability of **Pt1-NHS** in PBS buffer (pH 7.4) overtime.

5. Photostability

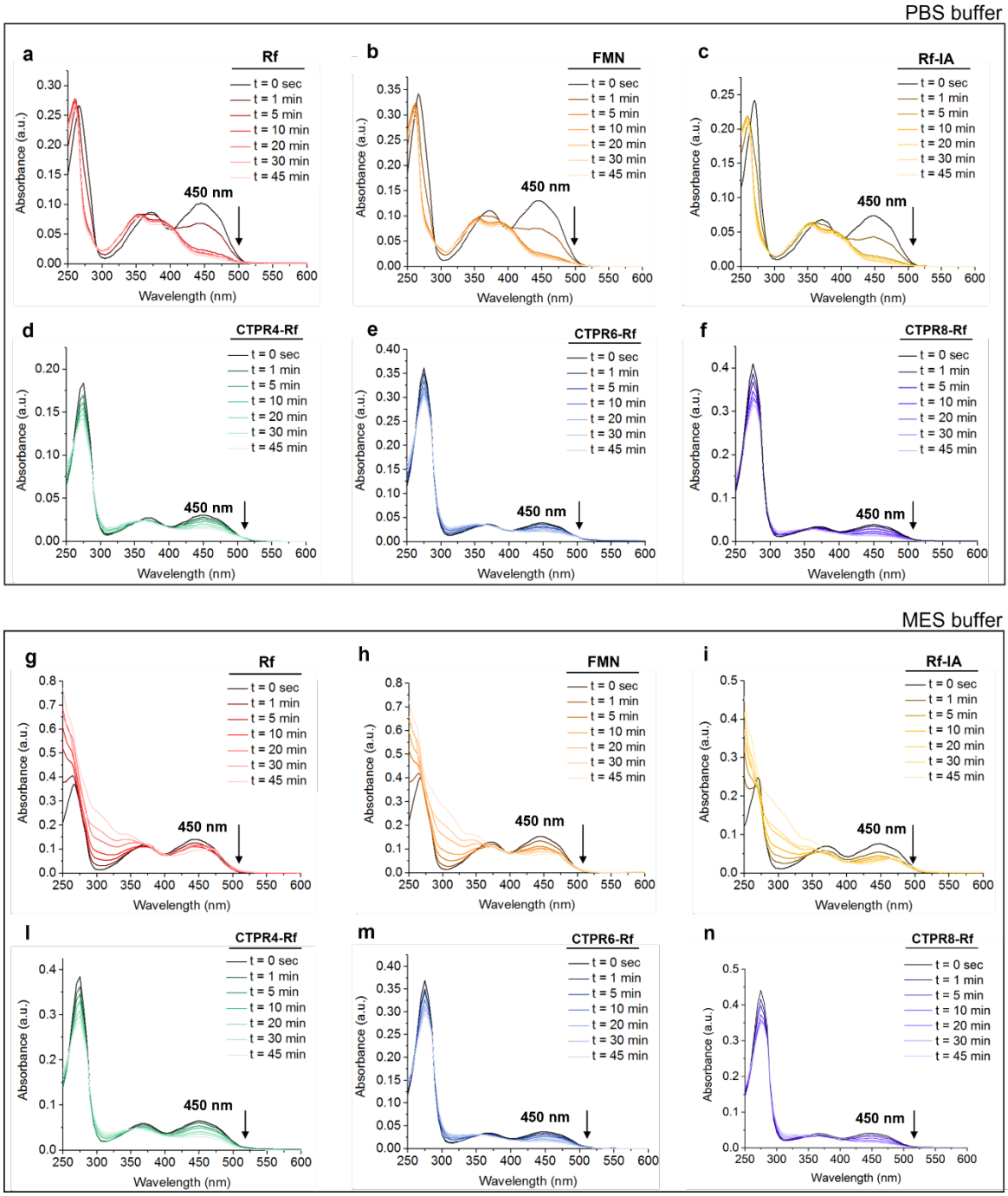

Fig. S8 Photostability of **Rf**, **FMN**, **Rf-IA** and **CTPR$_n$-Rf** in (a-f) PBS (140 mM NaCl, 50 mM phosphate buffer pH 7.4) and (g-n) MES buffer (18 mM, pH 6.4) under blue light irradiation (460 nm, 3.5 mW/cm^2).

6. Photocatalysis studies

Photocatalysis experiments

All photocatalysis experiments were monitored following the formation of the singlet signal, related to the release of the succinate for the reduction of the platinum complex. Here below is reported a schematic representation of **Pt2** photoreduction reaction:

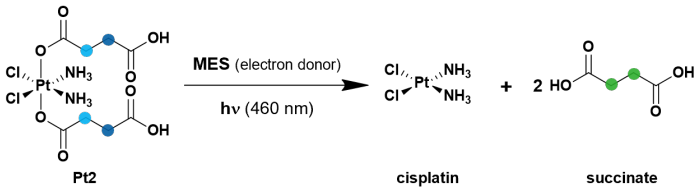

Photocatalysis tests were carried in a NMR tube with a total volume of 500 µL with the following composition: 500 µM platinum prodrug, 5 µM flavin catalyst, 7 µM and 12 µM substrate, 18 mM MES (pH 6.4) in 10% D_2O - 90% H_2O. Samples were irradiated with a custom-made array of blue light emitting diodes (460 nm, 3.5 mW/cm^2).

Integration of the free succinate ligand signal (2.25–2.35 ppm) was used for monitoring the reaction progress.

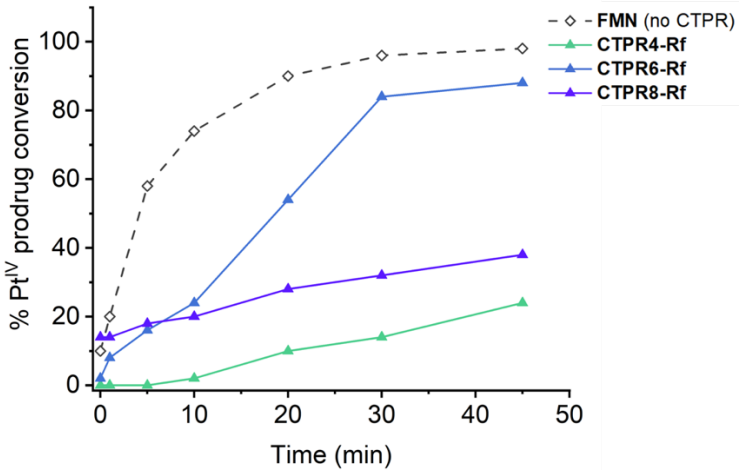

Fig. S9 Photocatalytic activation of free **Pt2** by **FMN**, **CTPR4-Rf**, **CTPR6-Rf** and **CTPR8-Rf**. Experimental conditions: [**Pt2**] = 500 µM, [**CTPR$_n$-Rf**]$_{Rf}$ = 5 µM, [**FMN**] = 5 µM, [MES] = 18 mM (pH 6.4), hν = 460 nm (3.5 mW/cm^2).

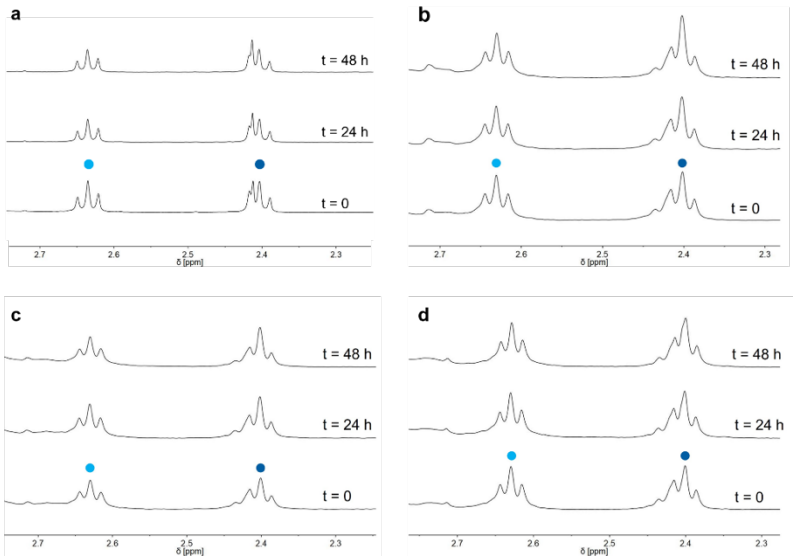

Fig. S10 Dark stability of **Pt2** in the presence of **FMN** and the protein-catalyst bioconjugate systems in MES buffer (10% D_2O): (a) **FMN**, (b) **CTPR4-Rf**, (c) **CTPR6-Rf**, (d) **CTPR8-Rf**.

Experimental conditions: [**Pt2**] = 500 µM, [**FMN**]= 5 µM, [**CTPR$_n$-Rf**]$_{Rf}$ = 5 µM, [**CTPR$_4$-Rf**]$_{CTPR4}$ = 7.6 µM, [**CTPR$_6$-Rf**]$_{CTPR6}$ = 12 µM, [**CTPR$_8$-Rf**]$_{CTPR8}$ = 7.7 µM, [MES] = 18 mM (pH 6.4), hν = 460 nm (3.5 mW).

^{1}H-NMR signal labeling: ● Pt-OCO**CH$_2$**CH$_2$CO$_2$H, ● Pt-OCOCH$_2$**CH$_2$**CO$_2$H, and ● free O$_2$C**CH$_2$CH$_2$**CO$_2$H.

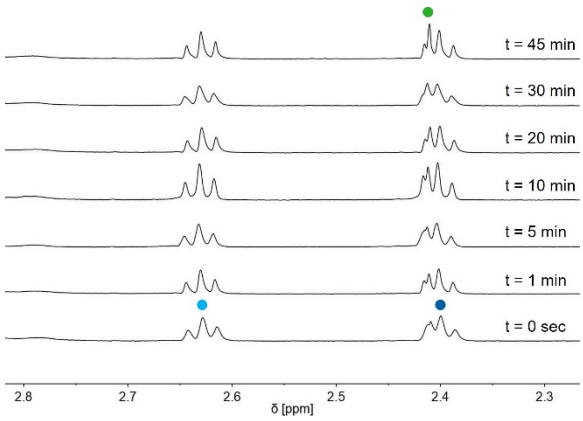

Fig. S11 Photocatalytic activation of **Pt2** complex in MES buffer (10% D_2O). Experimental conditions: [**Pt2**] = 500 µM, [MES] = 18 mM (pH 6.4), hv = 460 nm (3.5 mW/cm^2).

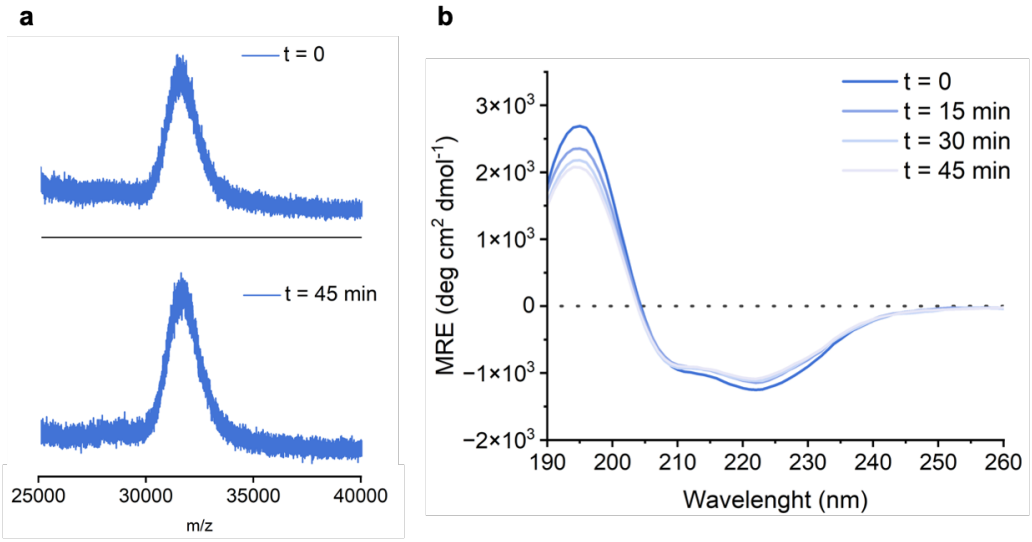

Fig. S12 Photostability of **CTPR6-Rf-Pt1**. (a) MALDI-TOF spectra of **CTPR6-Rf-Pt1** before (t = 0) and after 45 min of light irradiation (460 nm, 3.5 mW/cm^2). (b) CD spectra in PB buffer of **CTPR6-Rf-Pt1** at different irradiation times (460 nm, 3.5 mW/cm^2) in the spectral region of the protein secondary structure absorption.

7. Incubation experiments with GSH

The dark stability of **Pt1** and **CTPR6-Rf-Pt1** in the presence of the biological thiol L-glutathione (GSH) was investigated in comparison to cisplatin. **Pt1**, **CTPR6-Rf-Pt1,** and cisplatin (50 µM Pt) were incubated for 24 h with an excess of GSH (1:100) in aqueous solution at room temperature. The samples were monitored at three different time points: 0, 6 and 24 h using UPLC-MS.

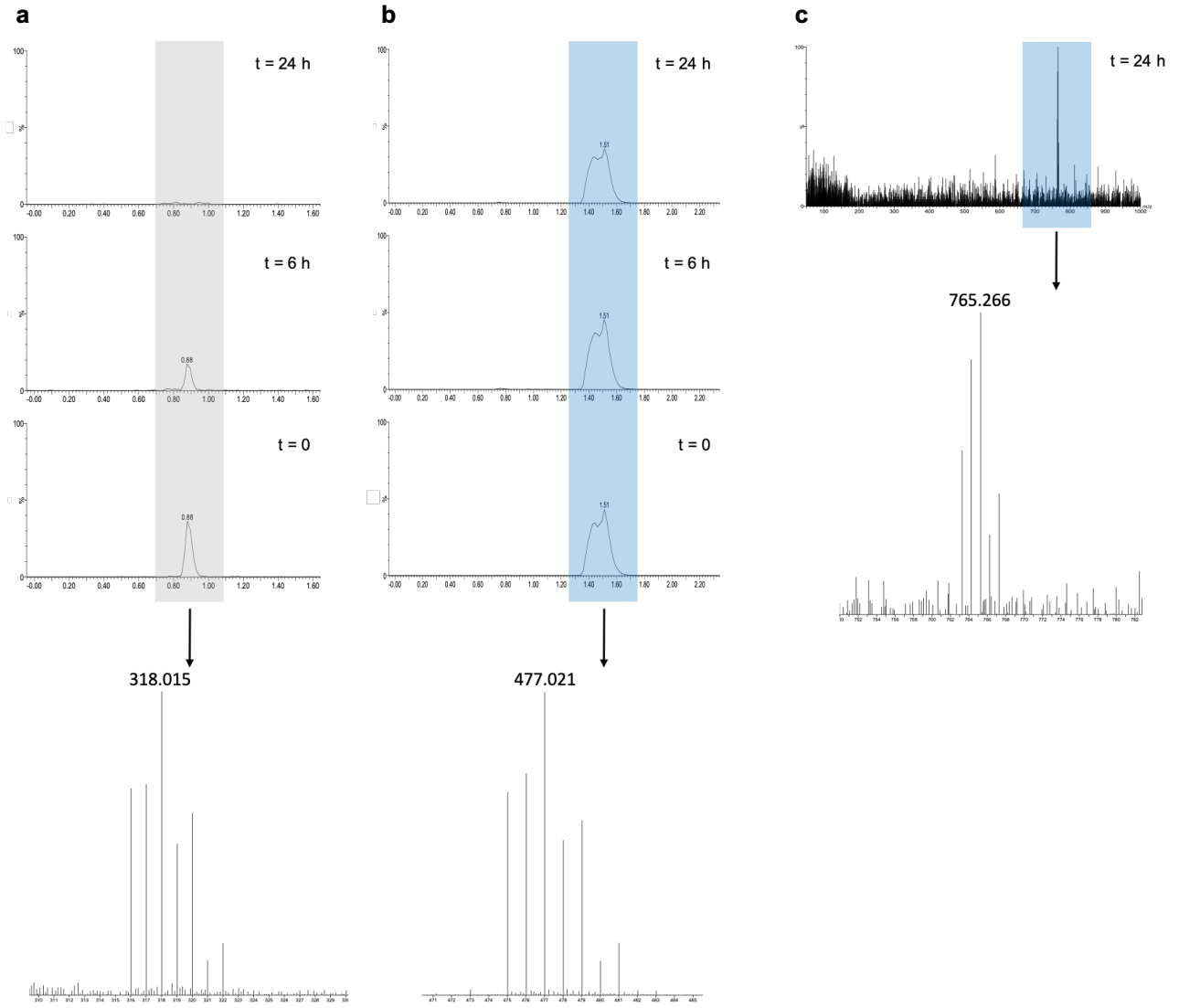

Fig. S13 (a) Dark stability of cisplatin (50 µM) co-incubated with GSH (500 µM) in water, monitored at 0, 6 h and 24 h: (top) UPLC chromatogram, (bottom) mass spectrum of the elution peak at 0.88 min (m/z = 318.015), corresponding to $[Pt(Cl)_2(NH_3)_2 + NH_4^+]$; (b) Dark stability of **Pt1** (50 µM) co-incubated with GSH (500 µM), monitored at 0, 6 h and 24 h: (top) UPLC chromatogram, (bottom) mass spectrum of the elution peak at 1.56 min (m/z = 477.021), corresponding to [**Pt1** + H^+]; (c) UPLC chromatograms for **CTPR6-Rf-Pt1** (50 µM) co-incubated with GSH (500 µM) at 0, 6 h and 24 h did not show any major MS peak corresponding to free Pt species. We could detect traces of a Pt species (m/z = 765.266) only for the 4.2 min elution peak after 24 h of incubation with GSH.

8. Cell Viability experiments

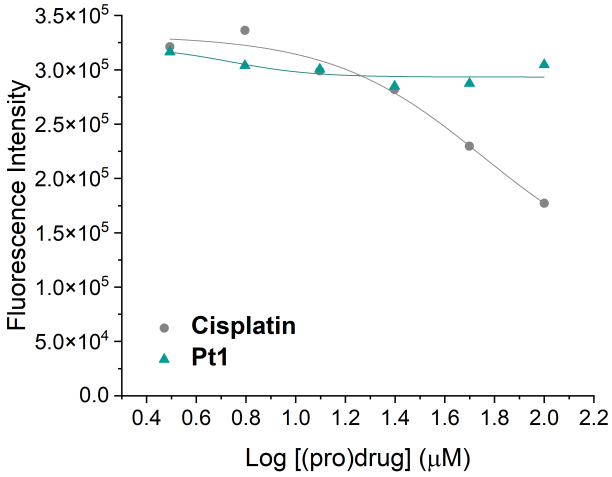

Fig. S14 Dose response curve of cisplatin and **Pt1** complex in PANC-1 cancer cell line. Experimental conditions for both metals: 3.12 μM, 6.25 μM, 12.5 μM, 25 μM, 50 μM, 100 μM. 24 hours uptake in dark, 37°C.

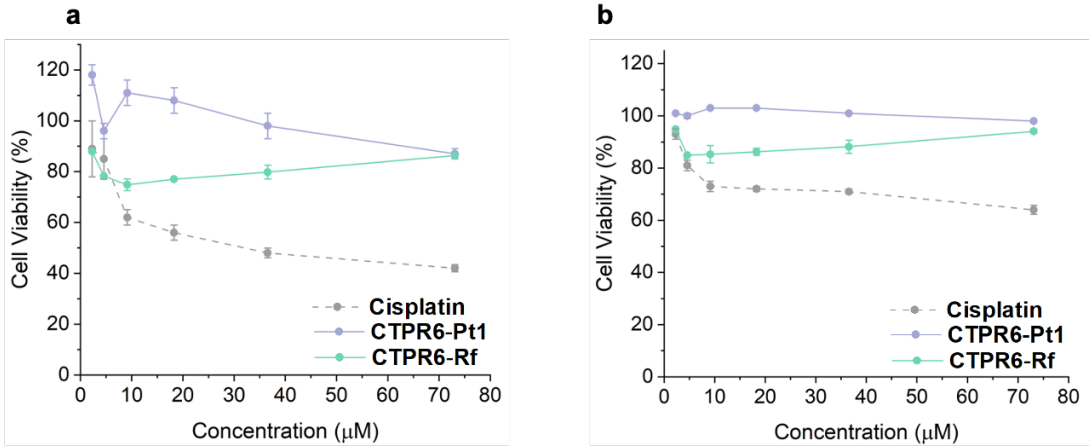

Fig. S15 Percentage cell viability in PANC-1 cancer cells following treatment with cisplatin (dashed line), **CTPR6-Pt1** (violet) and **CTPR6-Rf** (green) systems (a) under light irradiation (45 min, on/off regime 460 nm, 3.5 mW/cm^2) and (b) in dark conditions. The concentrations reported are related to the ones of drug/prodrug.

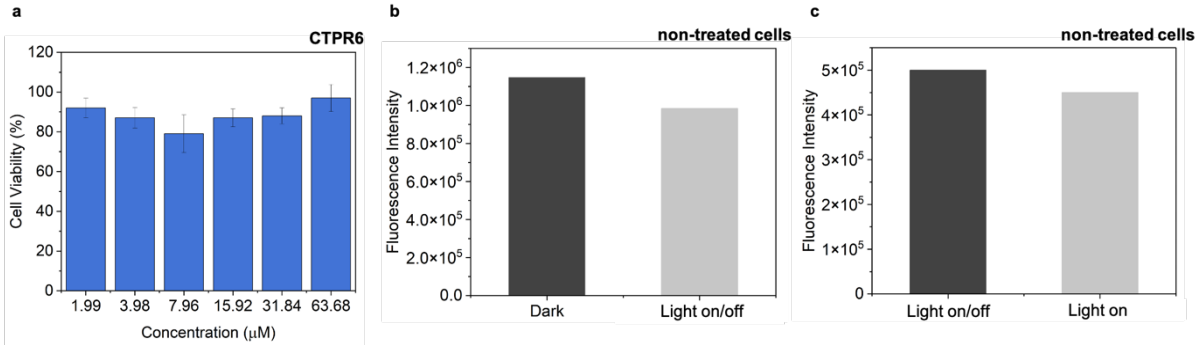

Fig. S16 (a) Cell viability percentage in PANC-1 cancer cells following treatment with **CTPR6** in dark condition. Experimental conditions: [**CTPR6**] = 1.99 μM, 3.98 μM, 7.96 μM, 15.92 μM, 31.84 μM, 63.68 μM. 24 hours uptake in dark, 37°C. (b) Fluorescence intensity of non-treated PANC-1 cancer cells in dark condition (dark gray) and under light on/off (light gray). The cells were irradiated for 45 min total, with blue light (3.5 mW/cm^2). (c) Fluorescence intensity of non-treated PANC-1 cancer cells with light on/off (dark gray) and with light on (light gray). The cells were irradiated for 45 min total, with blue light (3.5 mW/cm^2).

References

1 H. E. Gottlieb, V. Kotlyar and A. Nudelman, *J. Org. Chem.*, 1997, **62**, 7512–7515.

2 J. B. Metternich, S. Sagebiel, A. Lückener, S. Lamping, B. J. Ravoo and R. Gilmour, *Chem. Eur. J.*, 2018, **24**, 4228–4233.

3 A. Y.-T. Huang, C.-H. Tsai, H.-Y. Chen, H.-T. Chen, C.-Y. Lu, Y.-T. Lin and C.-L. Kao, *Chem. Commun.*, 2013, **49**, 5784.

4 J. Alguacil, S. Defaus, A. Claudio, A. Trapote, M. Masides and J. Robles, *Eur. J. Org. Chem.*, 2010, **2010**, 3102–3109.

5 C. Garino, S. Ghiani, R. Gobetto, C. Nervi, L. Salassa, V. Ancarani, P. Neyroz, L. Franklin, J. B. Alexander Ross and E. Seibert, *Inorg. Chem.*, 2005, **44**, 3875–3879.

6 R. A. Alderden, M. D. Hall and T. W. Hambley, *J. Chem. Educ.*, 2006, **83**, 728.

7 K. M. Brière, R. Goel, F. H. Shirazi, D. J. Stewart and I. C. P. Smith, *Cancer Chemother. Pharmacol.*, 1996, **37**, 518–524.

8 H. Yao, Z. Xu, C. Li, M.-K. Tse, Z. Tong and G. Zhu, *Inorg. Chem.*, 2019, **58**, 11076–11084.

9 M. Ravera, E. Perin, E. Gabano, I. Zanellato, G. Panzarasa, K. Sparnacci, M. Laus and D. Osella, *J. Inorg. Biochem.*, 2015, **151**, 132–142.

10 T. Kajander, A. L. Cortajarena and L. Regan, in *Protein Design*, Humana Press, New Jersey, 2006, vol. 340, pp. 151–170.

11 S. H. Mejías, J. López-Andarias, T. Sakurai, S. Yoneda, K. P. Erazo, S. Seki, C. Atienza, N. Martín and A. L. Cortajarena, *Chem. Sci.*, 2016, **7**, 4842–4847.

12 L. De Rosa, A. L. Cortajarena, A. Romanelli, L. Regan and L. D. D'Andrea, *Org. Biomol. Chem.*, 2012, **10**, 273–280.